Combinatorial testing of viral vector and CRISPR systems for precision genome editing

Li, Z.

Chapter 5

Selector AAV-CRISPR vectors purge off-target chromosomal insertions and promote precise genome editing

Zhen Li[1,*], Xiaoling Wang[1,*], Jin Liu[1], Josephine M. Janssen[1],

Rob C. Hoeben[1] and Manuel A.F.V. Gonçalves[1]

In preparation

* These authors contribute equally to this work

[1]Leiden University Medical Centre, Department of Cell and Chemical Biology, Einthovenweg 20, 2333 ZC, Leiden, The Netherlands.

Abstract

Adeno-associated viral (AAV) vectors are commonly used for genome editing owing to the proclivity with which their single-stranded genomes serve as homologous recombination (HR) substrates during programmable nuclease-assisted gene targeting. However, the high recombinogenic nature of recombinant AAV genomes also facilitates their non-homologous end joining at off-target chromosomal breaks ("capture") created by said nucleases, mutagens, or DNA metabolic processes. The collateral build-up of off-target and random insertions occurs in an AAV dose-dependent manner and greatly diminishes the overall genome-editing accuracy. Moreover, AAV donor constructs can equally yield imprecise on-target edits resulting from non-homologous recombination pathways. Here, we demonstrate that endowing AAV donors with marker-free selectable sequences permits enriching for cells precisely co-edited at target and endogenous *ATP1A1* alleles. These selector AAV donors instal *ATP1A1* polymorphisms conferring resistance to the small-molecule ouabain and, in the process, yield high frequencies of on-target and precisely edited cell populations independently of the initially applied vector dose (up to 99.4%). Crucially, we further report that next to marker-free enrichment for precisely edited cell populations, selector AAV donors achieve a thorough removal of cells with off-target DNA insertions heightening, therefore, the ultimate precision of AAV-based genome editing.

Introduction

Genome editing technologies are emerging at a fast pace with their application in scientific and biotechnological realms continuing to expand (Pacesa *et al*. 2024). Insertion of exogenous (donor) DNA at predefined chromosomal positions (gene targeting or knock-in) subjected to double-strand DNA breaks (DSBs) made by clustered regularly interspaced short palindromic repeat (CRISPR)-derived nucleases, forms a set of commonly used and highly versatile genome editing principles. This results from the amenability of these gene targeting approaches to large genomic edits (*e.g*.,

whole transgene knock-ins) and the straightforward programmability of RNA-guided CRISPR nucleases, such as those built on the prototypic CRISPR-Cas9 adaptive immune system from *Streptococcus pyogenes* (Pacesa et a. 2024). Engineered CRISPR-Cas9 nucleases, consisting of a sequence-tailored guide RNA (gRNA) and a Cas9 enzyme induce DSBs at DNA sequences that, next to a protospacer adjacent motif (*i.e*., NGG), have a *circa* 20-bp nucleotide tract (protospacer) complementary to the 5' end of the gRNA (spacer). Subsequent DSB repair by donor DNA substrates tailored for homology-directed repair mechanisms, *e.g*., homologous recombination (HR) (Liao *et al*. 2024) or for alternative DNA end-joining processes (He *et al*. 2016; Suzuki *et al*. 2016), results in targeted genome editing. Critically, when compared to donor constructs tailored for DNA end-joining processes, HR donors yield directional and more accurate gene knock-ins by mitigating insertions and mutations at, respectively, off-target positions and endogenous-exogenous DNA junctions (Liao *et al*. 2024; He *et al*. 2016). Unfortunately, HR-mediated genome editing is an inefficient process that often requires auxiliary measurers, *e.g*., addition of inhibitors of competing and dominant error-prone DNA repair pathways, like non-homologous end joining (NHEJ) and microhomology end joining (MMEJ) or, more typically, incorporation of selectable marker expression units in donor constructs to enrich for gene-edited cell fractions (Chu *et al*. 2015; Wimberger *et al*. 2023; Schimmel *et al*. 2023). However, interfering with endogenous DNA repair processes raises genomic instability concerns (Bischoff *et al*. 2020); whilst chromosomal insertion of heterologous marker genes limits the applicability and increases the complexity of gene editing protocols (Mikkelsen and Bak, 2023). Interestingly, the co-transfection of donor HR plasmids with selectable markers and genes-of-interest targeting independent loci permits drug-dependent enrichment for cells edited simultaneously at both loci, indicating the preferential isolation of HR-proficient cells amongst heterogeneous cell populations (Shy *et al*. 2016; Mitzelfelt *et al*. 2017). Building on this phenomenon, marker-free co-selection strategies have been devised where a

donor plasmid is co-transfected with a secondary donor construct or oligonucleotide designed for creating drug- or toxin-selectable dominant alleles with specific polymorphism(s) (Agudelo *et al*. 2017; Wiebking *et al*. 2020; Li *et al*. 2021). A marker-free co-selection strategy based on the acquisition of gain-of-function resistance to a highly potent and specific inhibitor of the sodium/potassium (Na^+/K^+) ATPase pump, namely the plant-derived cardiotonic steroid ouabain, constitutes a particularly powerful co-selection approach (Agudelo *et al*. 2017). The main attributes of this approach are two-fold. Firstly, it targets the essential and ubiquitously expressed *ATP1A1* gene yielding, as a consequence, a robust and universal selectable phenotype; and, secondly, it is based on a commercially available and cheap small-molecule that, over decades, has been administered for congestive heart failure (Wu *et al*. 2015). Moreover, distinct *ATP1A1* polymorphisms confer cellular resistance to a broad range of ouabain concentrations which can be exploited for reiterative implementation of distinct genomic edits within individual cells (Levesque *et al*. 2022).

Plentiful physical and chemical transfection methods allow for introducing genome editing reagents into human cells including donor DNA substrates in the form of plasmids or synthetic oligonucleotides. However, achieving optimal transfection efficiencies without the build-up of cytotoxic effects is demanding as it often requires systematic cell type-specific protocol optimizations. Moreover, the ultimate performance of these optimized protocols, whose reagents are sometimes unknown due to proprietary reasons, typically depends on subtle experimental conditions, *e.g*., cell-cycle stage distributions during transfection. In contrast to transfections, viral vector transductions present higher reproducibility and can be directly applied to different cell types independently of their cell cycle statuses. Valuable viral vector delivery properties stem from the fine-tuned mechanisms evolved by their wild-type counterparts in delivering nuclei acids into the cytoplasm or nucleus of the host cell. In this regard, commonly used adeno-associated viral (AAV) vectors with regular, pseudotyped or engineered capsids are

particularly effective sources of donor DNA in a broad range of mammalian cell types (Epstein and Schaffer, 2017). Moreover, AAV vector genomes consisting of single-stranded DNA flanked by hairpin-forming inverted terminal repeats (ITRs), are prone to HR when harbouring sequences identical to those framing programmable nuclease target sites. Indeed, AAV HR donors yield high-efficiency gene targeting including in human cells with potential and established therapeutic relevance (Epstein and Schaffer, 2017). Unfortunately, their recombinogenic nature also contributes to off-target and imprecise on-target chromosomal donor DNA insertions involving non-homologous recombination processes (Miller *et al*. 2004; Hanlon *et al*. 2019; Ferrari *et al*. 2022; Li *et al*. 2024). Other insidious byproducts include on-target and off-target chromosomal insertion of, respectively, concatemeric structures and heterogeneous AAV DNA species that often, harbour ITR sequences (Hanlon et a. 2019; Ferrari *et al*. 2022; Li *et al*. 2024; Suchy *et al*. 2024). The latter events raise transcriptome deregulation and insertional oncogenesis risks due to the known transcriptional competency of ITR elements (Ferrari *et al*. 2022; Flotte *et al*. 1992; Haberman *et al*. 2000; Bazick *et al*. 2024). Equally of concern, AAV genomes, possibly due to mimicking DNA lesions or repair intermediates, can impair cell viability through P53-dependent DNA damage response (DDR) activation whose consequences are particularly deleterious during stem-cell genomic engineering (Schiroli *et al*. 2019; Allen *et al*. 2022). Critically, imprecise and off-target byproducts as well as cytotoxic effects are strictly proportional to AAV vector amounts (Schiroli *et al*. 2019; Allen *et al*. 2022).

Besides the efficiency, additional key parameters of genome editing procedures include their specificity and accuracy or fidelity (Maggio and Gonçalves, 2015). The former corresponds to the relative levels of on-target to off-target donor DNA insertions; the latter relates to the proportions between precise and imprecise on-target editing events.

The performance of marker-free co-selection systems in the context of viral vector delivery is presently unknown. Moreover, their utility for purging genome-edited cell populations from off-target as well as imprecise on-target chromosomal insertions is also underexplored. To fill these knowledge gaps, in this study, we set out to investigate AAV donor constructs harbouring marker-free co-selection components (selector AAV vectors) allowing for ouabain-dependent enrichment for genome-edited cells (Agudelo *et al*. 2017). We demonstrate that combining selector AAV vectors with ouabain treatments, next to enriching for genome-edited cell populations, achieves concomitant elimination of imprecise on-target edits and off-target and/or random donor DNA insertions from said populations. Interestingly, selector AAV vector titration experiments revealed that the highest fold-enrichment factors of genome-edited cell fractions are associated with the lowest vector input amounts which are expected to be beneficial for alleviating AAV vector production costs, off-target donor insertions and P53-dependent DDR activation.

Results

To start investigating AAV-based genome editing involving marker-free ouabain co-selection (**Figure 1A**), we assembled the selector vector AAV-HR$^{S1.A1}$. This vector contains HR donor templates and matched gRNA units designed for CRISPR-Cas9-induced transgene insertion at the human *AAVS1* safer harbour locus (19q13.4-qter); and generation of *ATP1A1* alleles with the Q118R and N129D (RD) polymorphisms conferring resistance to ouabain (**Figure 1B**). The *AAVS1*- and *ATP1A1*-specific gRNAs are complementary to intronic sequences to mitigate NHEJ-mediated mutagenesis of target alleles and both HR templates and cognate gRNA units are packaged in single AAV particles to guarantee their co-delivery into individual cells. Amongst the increasing range of genome editing strategies, gene knock-in into genomic safe harbour loci remains a particularly flexible approach as it permits to, for instance, correct in a predictable and safe manner the phenotype(s) of recessive disorders regardless of their causative mutations (Pavani and

Amendola, 2021). The predictability and safety attributes result from a mitigation of insertional mutagenesis, transgene silencing and/or variegated expression normally associated with genome engineering systems yielding semi-random and random integration profiles, *e.g.*, retroviral vectors and transposons, respectively.

Mock-transfected HeLa cells and HeLa cells transfected with a plasmid expressing Cas9 were transduced with AAV-HR$^{S1.A1}$ and, after sub-culturing in the presence or absence of ouabain, each population was subjected to clonal analysis for the characterization of genome editing events at *AAVS1* and *ATP1A1*. The former characterization involved junction PCR analysis; the latter entailed restriction fragment polymorphism (RFLP) assays (**Figure 1C**). EGFP-directed flow cytometry at 20 days post-transduction revealed that incubating in ouabain cells initially exposed to Cas9 led to a 2.8-fold increase in the frequency of stably transduced cells, hence, genetically modified cells (**Figure 1D**). Of notice, amongst the HeLa cell cultures not exposed to Cas9, those untreated with ouabain contained a measurable amount of stably transduced cells (2.3%), whilst those treated with ouabain, as expected, died (**Figure 1D**). Albeit at low frequencies, there are precedents for programmable nuclease-free gene targeting using AAV HR donors (Spector *et al*. 2021; Biijani *et al*. 2022) as well as for a role of inverted repeats, including the AAV ITR, in HR stimulation (Holkers *et al*. 2012). Yet, the exclusive AAV-HR$^{S1.A1}$ delivery setup suggests, nonetheless, that the vast majority of stably transduced cells contained random or off-target donor DNA insertions, hence wild-type *ATP1A1* alleles, in that they were readily eliminated by ouabain (**Figure 1D**). Importantly, combining AAV-HR$^{S1.A1}$ with Cas9 delivery resulted in an ouabain-dependent 2.8-fold increase in the frequency of stably transduced cells, suggesting selection for *AAVS1*-targeted cells (**Figure 1D**). Independent experiments involving HeLa cells initially transfected with plasmids expressing Cas9 or an inactive dCas9 protein and, subsequently, equally transduced with AAV-HR$^{S1.A1}$, yielded similar results, *i.e.*, ouabain-dependent elimination and enrichment of stably transduced cells

generated by AAV-HR$^{S1.A1}$ delivery alone and together with Cas9, respectively (**Supplementary Figure S1**).

As aforementioned, next to the efficiency, the specificity and accuracy of donor DNA integration are key parameters of genome editing procedures based on HR or otherwise. The specificity is defined by the presence of donor DNA at the target site whilst the accuracy results from generating seamless telomeric-sided and centromeric-sided junctions between exogenous and endogenous DNA (jT and jC, respectively). Therefore, to determine the specificity and accuracy of selector AAV-based genome editing in the presence and absence of ouabain, junction PCR screens were performed on isolated EGFP-positive cell clones, each of which representing individual genome-modifying events. Of notice, differently from splice acceptor gene-trapping and protein-tagging constructs, clonal isolation based on transcriptionally autonomous transgenes, such as that in AAV-HR$^{S1.A1}$, prevents the biased selection for on-target events. The screening of 160 randomly isolated clones (80 expanded with ouabain and 80 without), identified genome-modifying events corresponding to random or off-target donor DNA insertions (jT-/jC-), precise HR-mediated *AAVS1* gene targeting (jT+/jC+), partial gene targeting (jT+/jC- or jT-/jC+), and non-homologous recombination, namely, containing differently-sized amplicon(s) diagnostic for imprecise DNA end-joining events (**Figure 1E**, left panel, red, cyan, orange and yellow arrowheads, respectively; and **Supplementary Figure S2**). Moreover, ouabain selection led to a remarkable increase in the number of *ATP1A1* gene editing as traced through RFLP assays (**Figure 1E**, right panel and **Supplementary Figure S2**).

Significantly, when compared with untreated cultures, cultures treated with ouabain contained substantially lower amounts of imprecisely edited cells (**Figure 1F**, top panel). Indeed, all the three categories representing imprecisely edited cells were smaller in ouabain-treated cultures (**Figure 1F**, top panel; and **Supplementary Figure S2**). The substantial enrichment for

AAVS1-targeted and precisely edited cells in the presence of ouabain was paralleled by a remarkable expansion of *ATP1A1*-edited cells as assessed by RFLP assays (**Figure 1F**, bottom panel; and **Supplementary Figure S2**). This data demonstrates that besides enriching for gene-targeted cell fractions in an ouabain-dependent manner, selector AAV-HR$^{S1.A1}$ construct deployment is valuable for purging said fractions from off-target and/or imprecise genome editing byproducts. These results further support the robust ouabain-resistance phenotype conferred by installing the RD polymorphisms at *ATP1A1*.

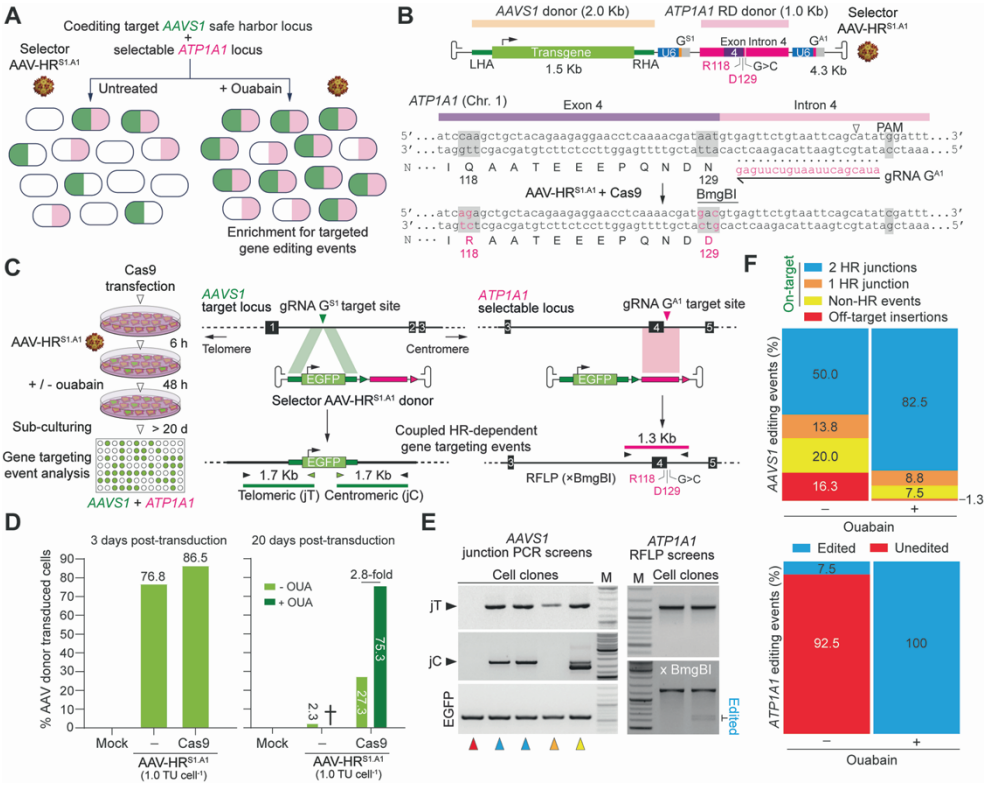

Figure 1. Testing and characterizing selector AAV genome editing at *AAVS1* and *ATP1A1*. (**A**) The marker-free co-selection principle. The cell population fraction whose intracellular milieu is conducive for HR (*e.g.*, cells undergoing the late G2/S phases of the cell cycle), are prone to simultaneous HR-mediated editing at two independent loci. As corollary, cells co-edited at a target sequence of interest and at a secondary selectable locus

can be enriched for when the latter locus acquires an edit(s) conferring a dominant resistance to a small-molecule drug. In this study, AAV-based genome editing of target and selectable *ATP1A1* alleles is assessed in the presence and absence of ouabain, a highly potent and specific inhibitor of the essential Na^+/K^+ ATPase pump. (**B**) Schematics of selector AAV donor construct and selectable *ATP1A1* site. The vector AAV-$HR^{S1.A1}$ contains *AAVS1* and *ATP1A1* donor templates and cognate matched gRNA units that, in the presence of Cas9, trigger HR-mediated chromosomal insertion of a transgene and polymorphisms at the former and latter loci, respectively. The *ATP1A1* polymorphisms Q118R and N129D (RD) confer resistance to ouabain. *ATP1A1* editing can be probed via restriction fragment length polymorphism (RFLP) assays using BmgBI in untreated and ouabain-treated cell populations. (**C**) Schematics of the experimental setup. Cas9-transfected HeLa cells are transduced with selector AAV-$HR^{S1.A1}$ donor and, after sub-culturing in the presence or absence of ouabain, are subjected to EGFP-directed flow cytometry and to clonal screens using junction PCR analysis and RFLP assays at *AAVS1* and *ATP1A1*, respectively. (**D**) Quantification of selector AAV donor delivery and DNA editing. HeLa cells subjected or not to Cas9 plasmid transfections were transduced with AAV-$H^{S1.A1}$ at 1 TU $cell^{-1}$. Donor delivery was assessed 3 days later by flow cytometry (left graph). After 20 days of sub-culturing in the presence and absence of ouabain, flow cytometry established AAV stable transduction frequencies (right graph). The cross indicates complete cell death in ouabain-treated cultures exposed exclusively to AAV-$HR^{S1.A1}$. (**E**) Characterization of genome editing outcomes. Left panel, representative clones yielding *AAVS1* amplicons diagnostic for gene targeting involving precise HR events at the telomeric and centromeric side of the target sequence are marked by cyan arrowheads (jT and jC, respectively). Representative clones lacking *AAVS1*-specific insertions (off-target), containing HR-independent targeted insertions and with only one HR-derived junction between transgenic and *AAVS1* sequences are marked by red, yellow, and orange arrowheads, respectively. Right panel, representative *ATP1A1* amplicons resistant and susceptible to BmgBI digestion diagnostic for unedited and edited *ATP1A1* alleles, respectively, are also depicted. (**F**) Cumulative characterization of genome editing outcomes. The frequencies of the different types of genome-modifying events detected in cell clones randomly isolated from HeLa cell populations stably transduced with AAV donor DNA and expanded in the presence or absence of ouabain are plotted (**Supplementary Figure S2**).

Recently, we introduced and characterized a dual viral vector genome-editing system based on the delivery of CRISPR-Cas9 nucleases and donor DNA templates via high-capacity adenovector particles (AdVPs) and AAV vectors, respectively (Li *et al*., 2024). Earlier experiments from our laboratory and those of others have shown that, contrary to linear free-ended DNA, capped double-stranded DNA, including adenovector genomes, are refractory to end-joining processes underpinning off-target and random chromosomal DNA insertions (Holkers *et al*. 2014; Medert *et al*. 2023). Moreover, besides their vast packaging capacity (*i.e.*, up to 36 kb), viral gene-free AdVPs display a remarkably lower cytotoxicity profile when compared to that of their viral gene-containing, earlier-generation, counterparts (Li *et al*. 2024; Brescia *et al*. 2020; Tasca *et al*. 2020; Ricobaraza *et al*. 2020). Hence, to expand and streamline the testing of selector AAV vectors in established cell lines as well as in difficult-to-transfect primary cells, we used this dual viral vector platform in HeLa cells and human mesenchymal stem cells (hMSCs). Initial co-transduction experiments in HeLa cells using AdVP.C9^{KARA}, a vector encoding the high-specificity nuclease SpCas9^{KARA} (**Figure 2A**) (Wang *et al*. 2021), and different amounts of AAV-HR$^{S1.A1}$, led to a clear dose-dependent increase in productive AAV transduction as assessed by EGFP-directed flow cytometry at 3 days post-transduction (**Figure 2B**). The significant AdVP.C9^{KARA}-dependent enhancement on productive AAV-HR$^{S1.A1}$ transduction (**Figure 2B**) is mostly caused by the higher transgene expression levels resulting from the buildup of chromosomally targeted templates over non-integrated episomes known to be prone to cellular restriction factors (Li *et al*., 2024; Dever *et al*. 2016). Moreover, earlier experiments have also established a causal relationship between CRISPR-Cas9-induced DSBs and productive AAV transduction (Li *et al*. 2024). Most importantly, after a 20-day sub-culturing period in the presence and absence of ouabain, EGFP-directed flow cytometry revealed significantly higher frequencies of stably transduced cells in the presence of ouabain (**Figure 2C**). Of notice, the lowest and highest stably transduced cell fold-enrichment factors were associated

with the highest and lowest AAV-HR$^{S1.A1}$ dosages, respectively (**Figure 2C**). Junction PCR and RFLP analyses (**Figure 2A**) of genomic DNA from stably transduced cell populations established ouabain-dependent co-selection of cells edited at *AAVS1* and *ATP1A1* (**Figure 2D**).

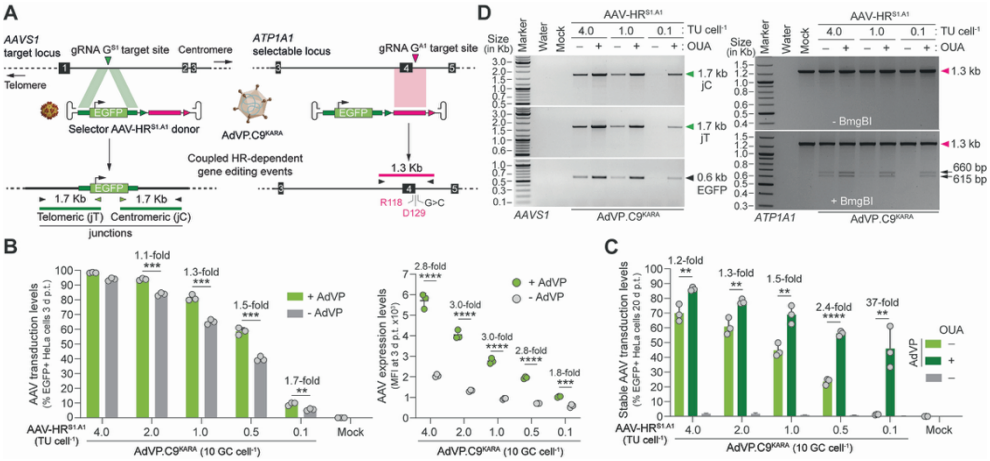

Figure 2. Selector AAV gene targeting at *AAVS1* and *ATP1A1* using combinatorial viral vector delivery. (**A**) Schematics of the experimental setup. Selector AAV-based gene targeting upon co-transduction of HeLa cells with vector AAV-HR$^{S1.A1}$, encoding donor and gRNA sequences, and vector AdVP.C9^{KARA}, encoding a Cas9 nuclease, was assessed via EGFP-directed flow cytometry and genotyping assays based on junction PCR and RFLP assays as depicted. (**B**) Quantification of selector AAV donor delivery. HeLa cells were transduced with AAV-HR$^{S1.A1}$ alone or together with AdVP.C9^{KARA} at the specified multiplicities of infection (MOI). Transduction levels were determined by flow cytometric quantification of EGFP-positive cell frequencies and respective mean fluorescence intensity (MFI) values at 3 days post-transduction (left and right graphs, respectively). Mock-transduced cells provided for negative controls. (**C**) Quantification of selector AAV-based DNA editing with and without ouabain. AAV stable transduction frequencies were measured via EGFP-directed flow cytometry after sub-culturing HeLa cells initially exposed to the indicated vector doses for 20 days. During sub-culturing, the cells were incubated or not with ouabain. Mock-transduced cells and cells transduced exclusively with AAV-HR$^{S1.A1}$ served as controls. The results are presented as mean ± SD of three biological replicates. Significant differences amongst the marked datasets were calculated by Student's t-tests; $^{**}P<0.05$. (**D**) Genotyping of *AAVS1* and *ATP1A1* in co-

transduced cell populations. *AAVS1* and *ATP1A1* gene editing in HeLa cells co-transduced with the indicated vectors and incubated or not with ouabain was assessed through junction PCR and RFLP assays (left and right panels, respectively). Mock-transduced cells provided for negative controls.

To test genome editing at an independent target locus, the selector AAV-HR$^{LMN.A1}$ donor was applied to HeLa cells and to primary hMSCs together with AdVP.C9^{KARA} (**Figure 3** and **Supplementary Figure S3**, respectively). The AAV-HR$^{LMN.A1}$ vector contains the same selectable sequence of AAV-HR$^{S1.A1}$ together with a *LMNA*-specific gRNA unit and a matched HR template for tagging LMNA at its N-terminus with the live-cell reporter mScarlet-I (**Figure 3A**). Of note, *LMNA* mutations have been linked to, amongst others, Emery-Dreifuss muscular dystrophy, limb girdle muscular dystrophy, dilated cardiomyopathy, and Hutchinson-Gilford progeria syndrome. In contrast to the use of autonomous transgene expression units, gene tagging setups are contingent on precise gene knock-in to guarantee expression from endogenous *cis*-acting regulatory elements. As such, this setup directly traces and quantifies HR-mediated gene editing events. Co-transductions targeting *LMNA* alleles broadly recapitulated the results obtained through experiments targeting the *AAVS1* locus (**Figure 2**). In particular, reporter-directed flow cytometry (**Figure 3B** and **Supplementary Figure S3A**), together with junction PCR and RFLP assays (**Figure 3C**, left and right panel, respectively) demonstrated an ouabain-dependent co-selection for cells edited at target *LMNA* and *ATP1A1* alleles. Again, the lowest and highest gene editing fold-enrichment factors resulted from applying the highest and lowest selector AAV doses, respectively (**Figure 3B** and **Supplementary Figure S3A**). The highest fold-enrichment factor (30-fold) was, in fact, observed in hMSCs initially co-transduced with AdVP.C9^{KARA} and AAV-HR$^{LMN.A1}$ at 500 GC cell^{-1} (**Supplementary Figure S3A**). These results indicate the feasibility in generating high frequencies of genome-edited cell populations while using low amounts of AAV vectors known to trigger dose-dependent cytotoxic effects in cell types with

therapeutic relevance, *e.g.*, stem cells. Further consistent with precise gene editing, direct fluorescence microscopy revealed that mScarlert::LMNA fusion products were present and properly located in cell nuclei exclusively in cultures exposed simultaneously to CRISPR-Cas9 and donor DNA reagents (**Figure 3D** and **Supplementary Figure S3B**). Finally, RFLP assays on unsorted cells and on mScarlet-positive and mScarlet-negative cells, further confirmed the strict ouabain-dependent selection of the *ATP1A1* RD variant. The strong positive selection for this endogenous marker gene is in fact particularly evident in cultures of mScarlet::LMNA-negative cells treated with ouabain (**Figure 3E**).

Taken together, the above-described experiments demonstrate that combining ouabain with tailored selector AAV vectors achieves a strong elimination of cells with imprecise on-target edits and off-target exogenous DNA insertions from CRISPR-edited cell populations. However, although the co-delivery of selectable *ATP1A1* and target donor sequences in single AAV vectors guarantees the presence of both donor templates in individual cells, at low vector doses, bipartite donor availability at primary and secondary loci is expected to become limiting. This consideration is supported by the decreasing ouabain-dependent genome editing frequencies at primary target loci as a function of diminishing AAV vector amounts, *i.e.*, at *AAVS1* safe harbour and *LMNA* loci (**Figure 2C** and **Figure 3B**).

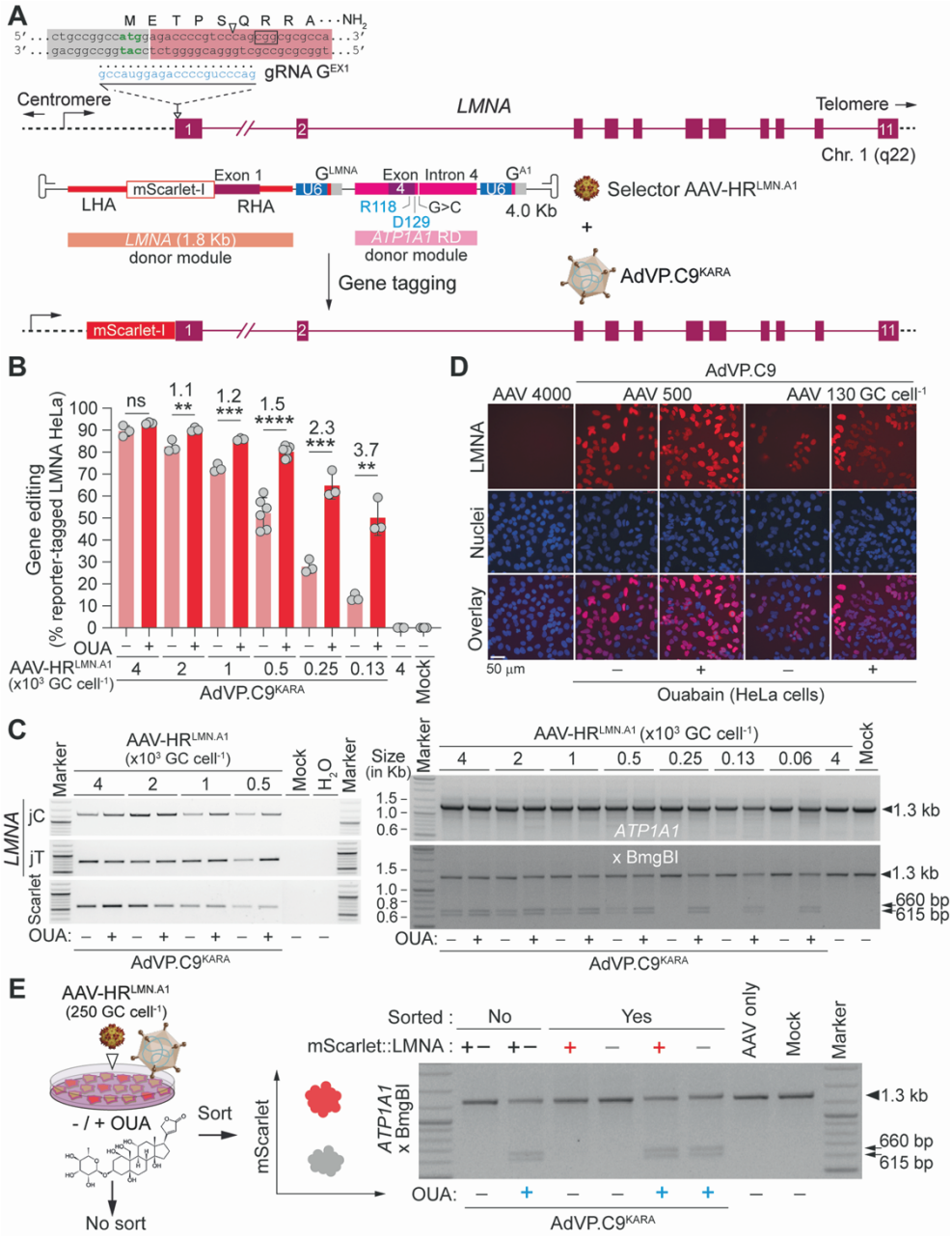

Figure 3. Selector AAV gene editing at *LMNA* and *ATP1A1* using combinatorial viral vector delivery. (**A**) Schematics of the experimental setup. Selector AAV-based gene tagging upon co-transduction of HeLa cells with AAV-HR$^{LMN.A1}$ donor and adenovector

AdVP.C9^{KARA} was monitored through mScarlet-directed flow cytometry and genotyping assays based on junction PCR and RFLP assays (not shown). (**B**) Quantification of selector AAV gene tagging with and without ouabain. Gene tagging was determined in HeLa cell populations initially exposed to the indicated vector doses via mScarlet-directed flow cytometry at 14 days post-transduction. Mock-transduced cells and cells transduced exclusively with AAV-HR$^{S1.A1}$ at 4,000 GC cell^{-1}, served as negative controls. The data are shown as mean ± SD of three biological replicates. Significant differences amongst the marked datasets were calculated by Student's t-tests; $^{**}P<0.05$. (**C**) Genotyping of *LMNA* and *ATP1A1* in co-transduced cell populations. *LMNA* and *ATP1A1* gene editing in HeLa cells co-transduced with the indicated vectors and incubated with or without ouabain was assessed through junction PCR and RFLP assays (left and right panels, respectively). Mock-transduced cells served negative controls. (**D**) Characterization of LMNA protein tagging. LMNA tagging and nuclear localization was monitored by combining direct fluorescence microscopy for mScarlet expression and nuclei labelling using the DNA dye Hoechst 33342. (**E**) Assessing ouabain-dependent selection of *ATP1A1* edited cells. HeLa cells co-transduced with AAV-HR$^{LMN.A1}$ and AdVP.C9^{KARA} and then cultured with or without ouabain were either sorted or not sorted to isolated LMNA-tagged positive and negative cells. *ATP1A1* editing in each cell population was probed through RFLP assays. Mock-transduced cells and cells exposed only to AAV-HR$^{LMN.A1}$ at 4,000 GC cel l^{-1}, served as negative controls.

Hence, we sought to investigate whether a more strict enrichment for genome-edited cells with sustained purging of random and/or off-target insertions is achievable by using selector AAV donors with transgenic DNA juxtaposed to a selectable polymorphism (**Figure 4A**). To this end, the vector AAV-HR$^{A1.IN17}$ was assembled (**Figure 4B**). This vector contains a gRNA unit for directing cleavage at intron 17 of *ATP1A1* and a matched donor DNA template designed for (i) *mScarlet-I* transgene knock-in at this intron; and (ii) installing the ouabain-selectable polymorphism T480N at the contiguous exon 17 (Agudelo *et al*. 2017). We started testing this selector AAV-HR$^{A1.IN17}$ vector with in-linkage transgene and T840N by transducing HeLa cells transfected with plasmids expressing Cas9 nuclease or Cas9^{D10A} nickase proteins. After sub-culturing in the presence or absence of ouabain, stably transduced cells were quantified by mScarlet-I-directed flow cytometry and

subjected to clonal analysis for characterizing genome-modifying events at the single-cell level (**Figure 4C**). At 3 days post-transduction, AAV-HR$^{A1.IN17}$ donor delivery into virtually all HeLa cells was achieved (**Figure 4D**, left panel). At 20 days post-transduction, ouabain untreated cultures initially exposed to Cas9 and Cas9^{D10A} had *circa* 60% and 7.4% of genome-modified cells, respectively (**Figure 4D**, right panel). This difference is consistent with single-strand DNA breaks (SSBs), or nicks, being generally weaker HR stimuli than DSBs (Chen *et al*. 2017), including when using AAV HR donors (Pavani *et al*. 2021). Despite this, nickase-based genome editing offers notable advantages that include a striking reduction in off-target effects and on-target allelic mutagenesis as, in contrast to DSBs, SSBs are typically not engaged by error-prone end joining repair pathways (Chen *et al*. 2017). Importantly, addition of ouabain to cultures transduced with AAV-HR$^{A1.IN17}$ and exposed to Cas9 or Cas9^{D10A} led to a significant increase in the frequencies of genome-modified cells, *i.e*., 1.6- and 12-fold, respectively (**Figure 4D**, right panel). Moreover, as previously observed when using the bipartite donor AAV-HR$^{S1.A1}$ (**Figure 1D** and **Supplementary Figure S1**), HeLa cell cultures exposed exclusively to AAV-HR$^{A1.IN17}$ contained a low, yet clearly measurable, proportion of stably transduced cells (3.5%). The selective abolishment of this cell fraction in the presence of ouabain (**Figure 4D**, right panel), indicates that it results from the random chromosomal insertion of vector DNA. In line with this, data from the subsequent junction PCR screening of 160 arbitrarily isolated mScarlet-positive clones (80 expanded from cultures exposed to Cas9 and 80 expanded from cultures exposed to Cas9^{D10A}), was consistent with the absence of randomly inserted donor DNA in cells grown in the presence of ouabain (**Figure 4E** and **Supplementary Figure S4**). Equally reminiscent of the results obtained with the bipartite donor AAV-HR$^{S1.A1}$ (**Figure 1F** and **Supplementary Figure S2**), next to off-target DNA insertion purging, combining ouabain incubation with in-linkage donor AAV-HR$^{A1.IN17}$ delivery also yielded a substantial reduction

of imprecise non-homologous recombination (**Figure 4E** and **Supplementary Figure S4**).

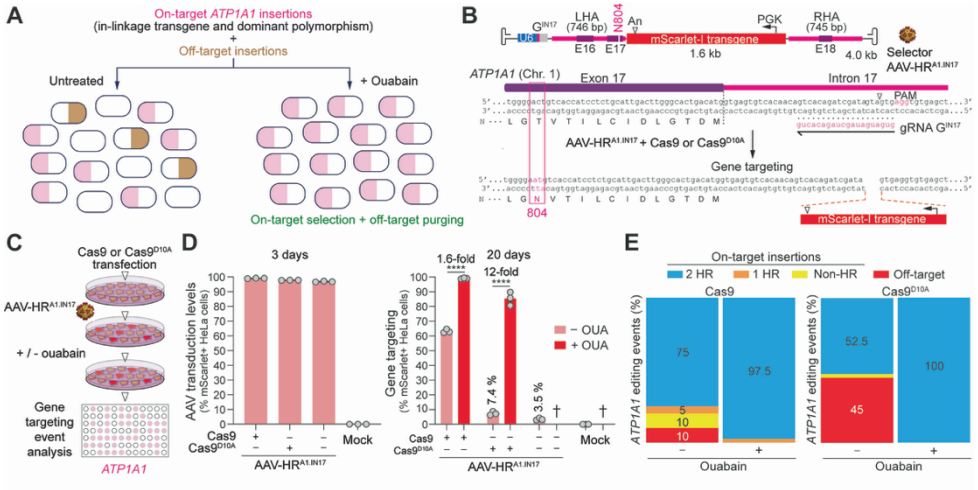

Figure 4. Testing and characterizing selector AAV genome editing based on gene knock-in and marker-free selection linkage. (**A**) Gene targeting with off-target insertions purging via gene knock-in and marker-free selection linkage. HR donors designed for concomitant knock-in of transgenes and dominant ouabain-resistance polymorphisms are postulated to achieve a strict enrichment for gene targeted cells with the simultaneous thorough eradication of random and/or off-target donor DNA insertions. (**B**) Selector AAV donor with in-linkage transgene and dominant polymorphism. The selector AAV-HR$^{A1.IN17}$ vector harbours a gRNA unit specific for intron 17 of *ATP1A1* and a matched HR donor whose region homologous to *ATP1A1* encodes the ouabain-resistance polymorphism T804N. LHA and RHA, "left" and "right" homology arms, respectively. (**C**) Schematics of the experimental setup. HeLa cells transfected with Cas9 nuclease or Cas9^{D10A} nickase constructs are transduced with AAV-HR$^{A1.IN17}$ and cultured in the presence or absence of ouabain. The frequencies of genome-modified cells and the characterization of genome editing events are subsequently assessed trough mScarlet-directed flow cytometry and clonal screens using junction PCR analysis at *ATP1A1*, respectively. (**D**) Quantification of selector AAV donor delivery and DNA editing. HeLa cells subjected to Cas9 and Cas9^{D10A} plasmid transfections were transduced with AAV-HR$^{A1.IN17}$ at 1 TU cell^{-1}. Donor delivery was assessed 3 days later by flow cytometry (left graph). After 20 days of sub-culturing in the presence and absence of ouabain, flow cytometry determined gene targeting frequencies (right graph). The crosses denote full cell death in ouabain-treated cultures exposed exclusively to AAV-HR$^{A1.IN17}$. (**E**) Cumulative

characterization of genome editing outcomes. The frequencies of the different types of genome-modifying events detected in cell clones randomly isolated from HeLa cell populations stably transduced with AAV-HR$^{A1.IN17}$ donor DNA and expanded in the presence and absence of ouabain are plotted. Gene targeting events derived from precise HR at the telomeric and centromeric side of the target sequence are marked in cyan. Gene targeting events involving partial HR or no HR are labelled in orange and yellow, respectively. Off-target donor DNA insertion events are coloured in red (**Supplementary Figure S4**).

To test the performance of the selector AAV in-linkage design in terms of its robustness for ouabain-dependent selection of gene targeted cells (**Figure 5A**), hMSCs and HeLa cells were co-transduced with AdVP.C9^{KARA} and AAV-HR$^{A1.IN17}$ (**Figure 5B** and **5C**, respectively). As aforementioned, the observed AdVP.C9^{KARA}-dependent enhancement on productive AAV transduction (**Figure 5B** and **5C**) is primarily caused by the higher transgene expression resulting from the accumulation of chromosomally targeted exogenous DNA, known to be more refractory to cellular restriction factors than non-integrated episomal DNA (Dever *et al*. 2016; Li *et al*., 2024). Critically, after a sub-culturing period in the presence and absence of ouabain, mScarlet-directed flow cytometry disclosed remarkably strong ouabain-dependent positive selection that consistently yielded over 90% of gene targeting frequencies independently of selector AAV vector doses and transduced cell type (**Figure 5D** and **5E**).

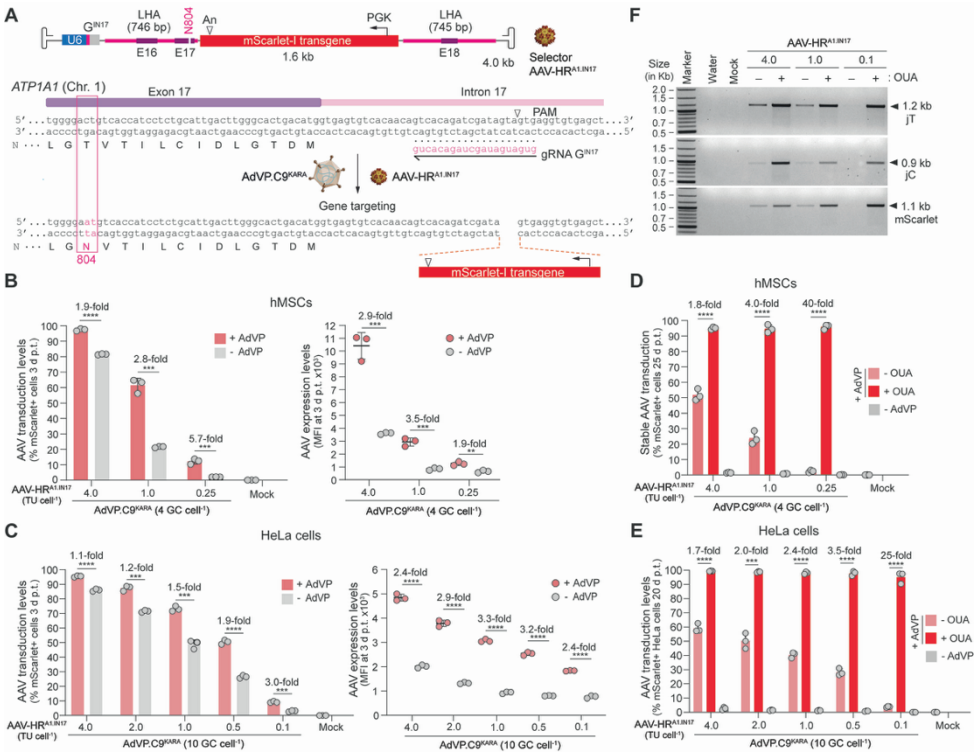

Figure 5. Selector in-linkage AAV gene targeting using combinatorial viral vector delivery. (**A**) Diagram of the experimental setup. The selector AAV-HR$^{A1.IN17}$ vector contains a gRNA unit specific for intron 17 of *ATP1A1* and a matched HR donor with the ouabain-resistance polymorphism T804N in its *ATP1A1* homologous region. LHA and RHA, "left" and "right" homology arms, respectively. (**B** and **C**) Quantification of selector AAV donor delivery. hMSCs and HeLa cells (panel B and C, respectively) were transduced with AAV-HR$^{A1.IN17}$ alone or together with AdVP.C9^{KARA} at the specified MOI. Transduction levels were determined by flow cytometric quantification of mScarlet-positive cell frequencies and respective MFI values at 3 days post-transduction (left and right graphs, respectively). Mock-transduced cells provided for negative controls. (**D** and **E**) Quantification of selector in-linkage AAV gene targeting with and without ouabain. Gene targeting frequencies in hMSC and HeLa cell cultures (panel D and E, respectively) were measured via mScarlet-directed flow cytometry after sub-culturing these cultures initially exposed to the indicated vector doses in the presence and absence of ouabain. Mock-transduced cells and cells transduced exclusively with AAV-HR$^{S1.A1}$ served as controls. The results are presented as mean ± SD of three biological replicates. Significant differences amongst the marked datasets were calculated by Student's t-tests; **P<0.05.

(**F**) Genotyping of *ATP1A1* in co-transduced cell populations. *ATP1A1* gene targeting in HeLa cells co-transduced with the indicated vectors and incubated or not with ouabain was assessed through junction PCR. Mock-transduced cells provided for negative controls.

Similarly to the bipartite donor AAV vectors co-targeting *ATP1A1* and *AAVS1* or *LMNA*, the lowest and highest stably transduced cell fold-enrichment factors were associated with the highest and lowest AAV-HR$^{A1.IN17}$ dosages, respectively (**Figure 5D** and **5E**). However, clearly, the in-linkage donor vector AAV-HR$^{A1.IN17}$ achieved a more thorough and homogeneous positive selection of gene targeted cells than that obtained with the bipartite donor vectors AAV-HR$^{S1.A1}$ and AAV-HR$^{LMN.A1}$. In fact, the highest fold-enrichment for gene targeted cells was obtained in hMSC cultures co-transduced with AdVP.C9^{KARA} and AAV-HR$^{A1.IN17}$ at 0.25 TU cell^{-1} where ouabain selection resulted in a 40-fold increase in the frequency of gene knock-ins (*i.e.*, 96±1.6% and 2.4±0.7% with and without selection, respectively) (**Figure 5D**). The purity levels for gene targeted cells in hMSC and HeLa cell cultures attained upon AdVP.C9^{KARA} and AAV-HR$^{A1.IN17}$ co-transductions and ouabain selection were consistently high, varying from a minimum of 94.6% to a maximum of 99.4% regardless of donor vector input amounts (**Figure 5D** and **5E**). Finally, junction PCR analysis of genomic DNA from stably transduced cell populations confirmed strict ouabain-dependent enrichment for *ATP1A1*-targeted cells (**Figure 5F**).

Taken together, these data establish the selector AAV in-linkage design as a robust strategy for achieving a strict selection for gene targeted cells through precise HR and, simultaneously, the purging of random and/or off-target donor DNA insertions from engineered cell populations.

Discussion

AAV vectors are commonly used in genome editing protocols as sources of donor HR substrates. However, the recombinogenic character of AAV vector genomes, that bear these substrates, fosters their “capture” at on-target and off-target or random chromosomal breaks through non-homologous end

joining processes (Miller *et al*. 2004; Hanlon *et al*. 2019; Ferrari *et al*. 2022; Li *et al*. 2024). Moreover, recent studies have demonstrated the pervasiveness of additional genomic DNA byproducts consisting of heterogeneous AAV vector-derived fragments and concatemeric species at off-target and on-target sites (Hanlon *et al*. 2019; Ferrari *et al*. 2022; Suchy *et al*. 2024; Li *et al*. 2024). The former AAV fragment intermediates, known to be packaged in vector particles (McColl-Carboni *et al*. 2024), typically contain transcriptionally-competent ITR elements (Flotte *et al*. 1992; Haberman *et al*. 2000), raising transcriptome deregulation and insertional oncogenesis concerns (Ferrari *et al*. 2022; Bazick *et al*. 2024). Finally, when combined with programmable nucleases, AAV vector genomes exacerbate P53 build-up and ensuing DDR activation that impairs cell viability in a strict vector dose-dependent manner (Schiroli *et al*. 2019; Allen *et al*. 2022).

We hypothesized that marker-free co-selection systems can be co-opted for addressing the aforementioned AAV-based genome editing shortcomings. These systems require neither chromosomal integration of exogenous selectable markers nor cell isolation reagents and equipment (*e.g*., FACS and MACS) (Mikkelsen and Bak, 2023). For this study, we selected a strategy based on ouabain, a highly potent and specific inhibitor of the ubiquitously expressed Na^+/K^+ ATPase pump (Agudelo *et al*. 2017). In contrast to other marker-free co-selection systems, such as that based on the potent inhibitor of mammalian protein synthesis diphtheria toxin protein, ouabain-dependent systems require a cheap small-molecule drug that has been used for congestive heart failure (Wu *et al*. 2015). Moreover, distinct *ATP1A1* polymorphisms confer resistance to a broad range of ouabain concentrations that can be exploited for sequential installation of distinct genomic edits (Levesque *et al*. 2022), including those underpinning regulatory systems, complex gene circuits and other synthetic biology devices. For instance, the herein tested polymorphisms T804N, located in the third extracellular loop, and Q118R/N129D located in the first extracellular loop of Na^+/K^+ ATPase, create variants resistant to ouabain inhibition at 10 μM and over 1000 μM,

respectively, in K562 cells (Levesque *et al*. 2022). Hence, after assembling AAV donor constructs endowed with matched gRNA units and ouabain-selectable sequences, we demonstrate that these selector AAV vectors, in addition to enriching for gene-targeted cell populations, achieve concomitant removal of imprecise HR-independent edits and off-target and/or random AAV donor DNA insertions. Interestingly, selector AAV vector titration experiments revealed that the highest fold-enrichment factors of gene-targeted cell fractions are associated with the lowest vector input amounts which are expected to be beneficial for alleviating both AAV production costs and detrimental P53-dependent DDR activation.

In this study, two types of selector AAV vector designs were investigated, namely, vector particles containing bipartite donor modules for *ATP1A1* and target gene co-editing, and vector particles bearing an in-linkage donor DNA module for direct *ATP1A1* targeting and selection. Selector AAV vectors with bipartite donors can be customized to implement distinct types of genomic edits (*e.g*., gene knock-ins, gene-tagging, or gene-repairing) at different loci, like the herein targeted *AAVS1* safe harbour locus and *LMNA* alleles. The former locus is a commonly used genomic landing pad for achieving homogenous and stable transgene expression (Lombardo *et al*. 2011; Pavani *et al*. 2021); the latter encodes lamin, a product found in the nuclear lamina matrix of proteins located underneath the inner nuclear membrane and whose mutations underpin, for instance, Emery-Dreifuss muscular dystrophy, limb girdle muscular dystrophy, dilated cardiomyopathy, Charcot-Marie-Tooth disease, and Hutchinson-Gilford progeria syndrome. However, although the co-delivery of selectable *ATP1A1* and donor sequences in single AAV vectors assures their presence in individual cells, at low vector doses, bipartite donor availability at primary and secondary loci should become limiting. This point is consistent with the observed gradual decrease in ouabain-dependent gene editing levels at primary target sequences as a function of diminishing AAV vector amounts.

Selector AAV vectors with in-linkage selecting and targeting donor templates are, on the other hand, restricted to creating gene knock-ins at *ATP1A1* alleles. Yet, *ATP1A1* can in principle serve as a suitable transcription-favourable genomic landing pad to, for instance, overexpress proteins in producer cells, control cell behaviour with synthetic gene circuits, or complement genetic defects in autologous patient-derived cells. Moreover, albeit less versatile than bipartite donors, selector AAV vectors with in-linkage selecting and targeting HR templates yield engineered cell populations with substantially higher degrees of purity for gene targeted cells independently of vector doses and transduced cell types (range: 94.6%-99.4%). Indeed, the ability to generate such high frequencies of gene targeted cells using low AAV vector doses should allow creating genome engineered cells with minimal risks of harboring off-target and/or random chromosomal insertion of exogenous DNA (intact or otherwise). These favorable selector AAV performance features might permit streamlining cell engineering efforts via bypassing the need for time-consuming cell line isolation and screening and, in addition, expand said efforts to cell types refractory to single-cell isolation and expansion, such as most primary cells whose proliferation is restricted by their Hayflick limit and ensuing senescence. Equally of note, selector AAV vectors with in-linkage donor designs require single instead of dual CRISPR-Cas9 nucleases, therefore reducing genomic instability risks. There is nonetheless a growing realization that especially in DNA damage sensitive cells, like stem cells, programmable nuclease-induced DSBs can be detrimental to target locus stability (Frock *et al*. 2015; Kosicki *et al*. 2018) and cell viability (Chen *et al*. 2017; Ihry *et al*. 2018; Schiroli *et al*. 2019). Significantly, research from our laboratory has demonstrated that, when compared with Cas9 nucleases, $Cas9^{D10A}$ nickases are substantially less disruptive to on-target and off-target sequences (Wang *et al*. 2021; Chen *et al*. 2020) and present greatly dampened P53-dependent DDR activation levels (Wang *et al*. 2023). Hence, the herein provided proof-of-principle that selector AAV-based genome editing is transportable to protocols involving

Cas9^{D10A}-induced HR is relevant for further refining and applying marker-free co-selection approaches.

In conclusion, in the present study, we integrate AAV HR donor delivery with a marker-free co-selection principle based on a commercially available and cheap small molecule, ouabain. We demonstrate that combining these selector AAV vectors with ouabain treatments, in addition to selecting for precisely edited cell populations, eradicates otherwise prevalent off-target and/or random AAV donor DNA insertions. Moreover, through selector AAV vector titration experiments, we report that the highest fold-enrichment levels for genome-edited cells is associated with the lowest vector inputs which is expected to be beneficial for mitigating AAV vector production costs and P53-dependent DDR activation processes known to limit AAV-based genome editing in DNA damage-sensitive cells. Selector AAV vectors are, therefore, expected to become useful in a broad array of basic and applied research contexts, such as for expediting cell engineering endeavours and generating well-defined populations of hard-to-transfect cell types including those that are refractory to clonal expansion but that hold nonetheless therapeutic relevance.

Materials and Methods

Cells

The human cervix carcinoma HeLa cells (ATCC) were cultured in high-glucose Dulbecco's modified Eagle's medium (DMEM; Thermo Fisher Scientific; Cat. No.: 41966-029) containing 5% fetal bovine serum (FBS; Biowest; Cat. No.: S1810-500). The HeLa cells were kept at 37°C in a humidified-air 10% CO_2 atmosphere. The primary human mesenchymal stem cells (hMSCs) were isolated from bone marrow and cultured in Minimum Essential Medium α (MEM-α; Thermo Fisher Scientific; Cat. No.: 22561-021) supplemented with 10% FBS, 100 U ml^{-1} penicillin/streptomycin (Thermo Fisher Scientific; Cat. No.: 15140-122), 1× non-essential amino acids (NEAA; Thermo Fisher Scientific; Cat. No.: 11140-050), 1× GlutaMax supplement

(Thermo Fisher Scientific; Cat. No.: 35050-061) and 5 ng ml^{-1} Recombinant Human Fibroblast Growth Factor-basic (FGF-2; Peprotech; Cat. No.: 100-18B). The hMSCs were kept at 37°C in a humidified-air 5% CO_2 atmosphere. The harvesting of these human primary cells was done following the Best Practices Code of the Dutch Federation of Biomedical Scientific Societies on anonymous surgery material remnants.

Recombinant DNA plasmids

The AAV transfer plasmids BI17_pAAV-$HR^{S1.A1}$, BI19_pAAV-$HR^{LMN.A1}$, and BI38_pAAV-$HR^{A1.IN17}$ were assembled by using standard recombinant DNA techniques. The complete nucleotide sequences and respective annotated maps of these constructs are available in the **Supplementary information.**

Recombinant AAV productions

Recombinant AAV particles were assembled on the basis of BI17_pAAV-$HR^{S1.A1}$, BI19_pAAV-$HR^{LMN.A1}$, and BI38_pAAV-$HR^{A1.IN17}$ as follows. HEK293T cells were seeded in T175-cm^2 culture flasks at a density of 2×10^7 cells per flask (up to 18 flasks per AAV vector stock) and, the next day, they were transfected with each AAV transfer plasmid (**Supplementary information**) together with the packaging plasmid AT51_pDG6.RSV.DsRed.SV40pA mixed at 1:1 molar ratios (30 µg total DNA per T175-cm^2 flask). This packaging plasmid expresses the AAV serotype-2 *rep* and AAV serotype-6 *cap* genes together with adenovirus helper functions, *i.e.*, VA RNAs I and II, E4ORF6, and E2A (Grimm *et al*. 2003).

Each T175-cm^2 culture flask received 99 µl of a 25-kDa linear polyethylenimine (PEI) solution (Polysciences) at 1 mg ml^{-1} and DNA mixtures, each diluted in 1 ml of 150 mM NaCl. These transfection mixtures were made by dropwise addition of the PEI to the DNA followed by direct homogenization in a vortex for 10 seconds. After 16-18 minutes at room temperature, the resulting DNA-PEI complexes were added to the HEK293T cells with the transfection medium being replaced 24 hours later by 20 ml of

culture medium. The HEK293T cell were detached at 5 days post-transfection by using a cell scrapper and collected into 50-ml tubes together with the conditioned medium. This material was then centrifuged at 1,000 ×*g* for 10 min at 4°C and the resulting supernatants and cell pellets were separately recovered and stored at -80°C until further processing. After thawing, 25 ml of a 40% (*w/v*) polyethylene glycol 8000 solution (PEG 8000; Sigma-Aldrich; Cat. No.: P2139) was added per 100 ml of supernatant with this mixture being first gently stirred for 1 hour at 4°C and subsequently stayed overnight at 4°C without stirring for particle precipitation. Next, the supernatant-PEG8000 mixtures were subjected to 2,820 ×*g* for 15 min at 4°C in 50-ml tubes after which the pellets were resuspended in 7 ml of PBS (pH 7.4) and mixed with 10 ml of clarified cell lysates to yield 17 ml of vector suspensions. The clarified cell lysates were generated by resuspending the producer-cell pellets in 10 ml of PBS (pH 7.4), subjecting the resuspended cells to three rounds of freezing and thawing using liquid N_2 and 37°C water baths, respectively, and eliminating cell debris via centrifugation at 3,220 ×*g* for 15 min at 4°C. The 17-ml AAV vector suspensions were then exposed to 50 U ml^{-1} of Benzonase (Millipore; Cat. No.: UFC910024) for 1 hour at 37°C and subsequently centrifuged at 2,420 ×*g* for 10 min at 4°C.

Recombinant AAV purification and characterization

The clarified supernatants harboring the AAV particles were then placed onto Iodixanol-OptiPrep (Progen; Cat. No.: 1114542) cushions of 15%, 25%, 40% and 60% in Quick-Seal round-top polypropylene tubes (Beckman; Cat. No.: 342414). The AAV vectors were purified through iodixanol gradient ultracentrifugation at 69,000 RPM in a 70Ti rotor (Beckman Coulter) at 16°C in a Beckman Coulter Optima XE-90 centrifuge. The ultracentrifuge tubes were pierced with a needle (18G needle BD Microlance™; Cat. No.: 304622) for recovering AAV vector particles in the 40% iodixanol cushion. The collected material was then subjected to buffer exchange using Amicon Ultra-15 100K MWCO filters (Millipore; Cat. No.: UFC910024) and Dulbecco's Phosphate-Buffered Saline (DPBS; Thermo Fisher Scientific; Cat. No.:

14040-091) containing 0.001% Poloxamer 188 (Sigma-Aldrich; Cat. No.: P5556). The purified batches of AAV-HR$^{S1.A1}$, AAV-HR$^{LMN.A1}$, and AAV-HR$^{A1.IN17}$ were stored at -80°C and their transducing unit (TU) titers were determined by end-point titrations on HeLa cells using flow cytometry or qPCR assays as readouts. For AAV-HR$^{S1.A1}$ and AAV-HR$^{A1.IN17}$ titrations, HeLa cells were seeded at a density of 5×10^4 cells per well of 24-well plates (Greiner Bio-One) and approximately 18 hours later, they were incubated with 3-fold serial dilutions of each vector batch. The frequencies of transduced cells were determined at 3 days post-transduction by EGFP- or mScarlet-directed flow cytometry with the functional AAV vector titers corresponding to TU per ml being determined as the percentage of transduced cells × number of cells seeded × dilution factor x 1000 μl^{-1}. The transducing titers of AAV-HR$^{LMN.A1}$, expressed in GC per ml, were determined via a qPCR assay based on the iQ SYBR Green Supermix (Bio-Rad, cat. No. L010171C) and the *mScarlet-I*-specific primers 5'-CTACCTGGCGGACTT CAAGA-3' and 5'-ACGGTGTAGTCCTCGTTGTG-3'. In brief, HeLa cells were seeded at 8.5×10^4 cells per well of 24-well plates (Greinder Bio-One) and, the next day, they were exposed to seven 3-fold serial dilutions of purified vector stock. Next, qPCR analysis was performed on genomic DNA isolated via the DNeasy Blood & Tissue kit at 24 hours post-transduction. In parallel, eight serial 10-fold dilutions of linearized parental AAV vector DNA containing 1×10^7 GC ml^{-1} served to setup a qPCR standard curve. Data analysis was done with the Bio-Rad CFX Manager 3.1 software (Bio-Rad Laboratories) and the titer was determined on the basis of the AAV vector DNA and plasmid Ct value standard curve.

Testing selector AAV genome editing at *AAVS1* and *ATP1A1*

HeLa cells were seeded at the density of 5×10^4 cells per well of 24-well plates. The next day, the cells were exposed or not to complexes formed by incubating 150 mM NaCl solutions containing 2.19 µl of PEI (1 mg ml^{-1}) and plasmid mixtures consisting of 420 ng of AV62_pU.CAG.Cas9.rBGpA or 420 ng AB66_pU.CAG.dCas9.rBGpA as negative control. To control for

transfection efficiency, all transfection mixtures were spiked with 80 ng of plasmid BE08_pCAG.mCherry.bGHpA expressing a red fluorescence-emitting reporter. After a 6-h incubation period, the medium of cells transfection-treated was removed, and the cells were transduced in regular culture medium containing AAV-HR$^{S1.A1}$ particles at 1 TU cell^{-1}. Ouabain selection of HeLa cells was initiated at 48 h post-trasdution with the concentration of 0.2 μM. HeLa cells were gone through flow cytometry at day 3 and day 20 to determine the transient and stable editing efficiencies, respectively, in the condition of ouabain selection or not.

Testing selector AAV in-linkage donor

HeLa cells were seeded 5 × 10^4 cells per well of 24-well plates. The next day, the cells were exposed or not to complexes formed by incubating 150 mM NaCl solutions containing 2.19 μl of PEI (1 mg ml^{-1}) and plasmid mixtures consisting of 420 ng of AV62_pU.CAG.Cas9.rBGpA, AB65_pU.CAG.Cas9 D10A.rBGpA, or AB66_pU.CAG.dCas9.rBGpA as negative control. To control for transfection efficiency, all transfection mixtures were spiked with 80 ng of plasmid AZ15_pU.CAG.eGFP.rBGpA expressing a green fluorescence-emitting reporter. After a 6-h incubation period, the medium of cells transfection-treated was removed, and the cells were transduced in regular culture medium containing AAV-HR$^{A1.IN17}$ particles at 1 TU cell^{-1}. Ouabain selection of HeLa cells was initiated at day 4 post-trasdution with the concentration of 0.2 μM. HeLa cells were went through flow cytometry at day 3 and day 20 to determine the transient and stable editing efficiencies, respectively, in the condition of Ouabain selection or not.

Viral vector transductions and DNA editing assays

HeLa cells and hMSCs were seeded at, respectively, 2×10^4 and 5×10^4 cells per well of 48- and 24-well plates (Greinder Bio-One) and, after overnight incubation, they were mock-transduced or were transduced for 24 hours with combinations of AdVP.C9^{KARA} (Li *et al*. 2024) and selector AAV vectors or with selector AAV vectors alone at the indicated MOIs. At 5- and 6-days post-

transduction, respectively, HeLa cells and hMSCs were cultured in the absence and in the presence of ouabain at final concentrations of 0.2 μM and 1.0 μM, respectively. Parallel cultures of mock-transduced cells were also exposed and not exposed to ouabain. Subsequently, genome modification endpoints were assessed at the indicated timepoints post-transduction by a combination of reporter-directed flow cytometry and *AAVS1*, *ATP1A1*, and *LMNA* genotyping analyses. The latter analysis involved RFLP and junction PCR assays whose details are specified in **Supplementary Tables S6 - S9**, **S12** and **S13**.

Microscopy analysis

The direct fluorescence microscopy analysis of reporter-tagged LMNA at early and late timepoints post-transduction was performed with an AF6000 LX inverted fluorescence microscope (Leica) and the resulting images were examined with the aid of the LAS X software (Leica Microsystems).

Flow cytometry analysis

Selector AAV vector transduction efficiencies and corresponding mean fluorescence intensities per cell were determined through reporter-directed flow cytometry using a BD LSR II FACS (BD Biosciences). The same apparatus was also used to quantify AAV stable transduction levels and *LMNA*-tagging frequencies. In brief, mock- and vector-transduced cells were rinsed with PBS (pH 7.4) and incubated in 0.05% trypsin-EDTA (Thermo Fisher Scientific; Cat. No.: 15400-054). The resulting cell suspensions were then collected in cultured medium, briefly centrifuged and resuspended in FACS buffer composed of PBS (pH 7.4) containing 0.5% (*w/v*) BSA and 2 mM EDTA (pH 8.0). The mock-transduced cells served to set the background fluorescence threshold cutoff. At least 10,000 viable single cells were acquired per sample. The resulting datasets were analyzed with the aid of the FlowJo 10.9.0 software (BD Biosciences).

Characterization of genome editing events

After sub-culturing selector AAV transduced cells for more than two weeks, reporter-positive cells were sorted by using either a BD FACSAria III flow cytometer (BD Biosciences) or a CytoFLEX SRT Cell Sorter (Beckman). Next, individual reporter-positive cells were seeded in wells of 96-well plates in 1:1 mixtures of culture medium and FBS supplemented with penicillin/streptomycin at 100 U ml^{-1} with or without 0.2 μM ouabain. Moreover, to increase cell cloning efficiencies, α-thioglycerol and bathocuprione disulphonate (both from Sigma-Aldrich) were added at final concentrations of 50 μM and 20 nM, respectively. Single cell-derived clones expressing reporter proteins were arbitrarily collected after 2-3 weeks for genotyping through junction PCR analyses using the Phire Tissue Direct PCR Master mix according to the manufacturer's instructions (Thermo Fisher Scientific; Cat. No.: F170L). The PCR mixture reagents and thermocycling parameters used in the clonal screens are indicated in the **Supplementary Tables S2 - S5**, **S10** and **S11**.

Statistical analyses

Statistical analyses were performed with the aid of the GraphPad Prism software (version 9.3.1) on datasets derived from a minimum of three biological replicates. Two-tailed unpaired Student's t tests were performed to assess statistical significance amongst two independent experimental groups. Details on statistical parameters are also indicated in the figure legends where applicable. P values inferior to 0.05 were considered to be statistically significant.

Acknowledgements

The authors are thankful to Thilo M. Buck and Jan Wijnholds (Department of Ophthalmology, Leiden University Medical Centre, The Netherlands) for their advice during the setting-up of AAV vector production procedures in our laboratory. The authors also thank the personnel of the Flow Cytometry Core Facility of the LUMC for aiding with the cell sorting procedures.

Authors in this study are members of the European Reference Network—Neuromuscular Diseases (ERN EURO-NMD).

Author contributions: Z.L. and X.W. generated and characterized reagents, designed and performed the experiments, examined the datasets and wrote the paper together with M.A.F.V.G.; J.L. generated, characterized and tested reagents; J.M.J. generated, characterized and tested reagents; R.H. supervised the research and analyzed the results; M.A.F.V.G. designed and supervised the research, analyzed the data and wrote the paper together with Z.L and X.W..

Funding

China Scholarship Council - Leiden University Scholarship to Z.L. and X.W.. Research in the author's laboratory is supported by the Prinses Beatrix Spierfonds, the Dutch Duchenne Parent Project, the Horizon Europe Programme, and the Dutch Research Council (NWO)—Open Technology Programme.

Conflict of interest statement

None declared.

Supplementary Figures

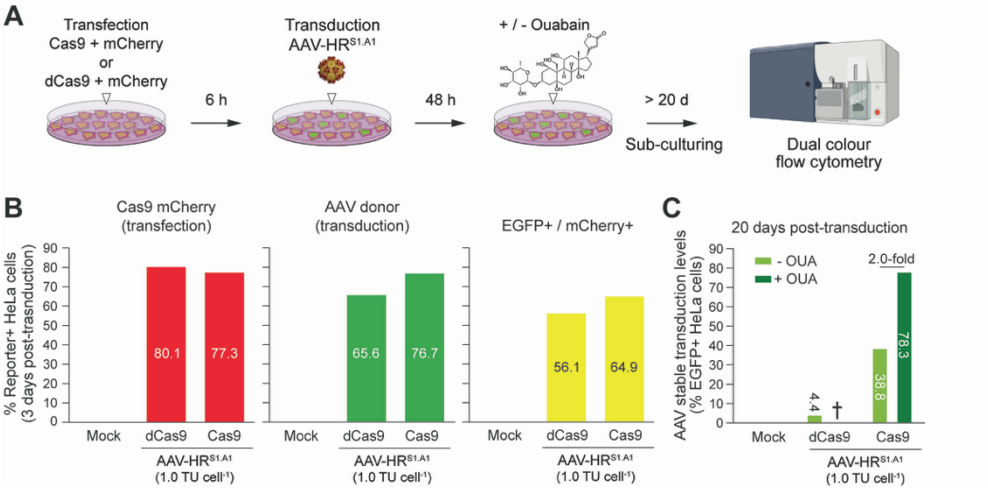

Supplementary Figure S1. Testing selector AAV-based genome editing at *AAVS1*. (**A**) Diagram of the experimental setup. HeLa cells transfected with plasmids expressing Cas9 and mCherry or inactive dCas9 and mCherry are transduced with the selector AAV-HR$^{S1.A1}$ donor and, after sub-culturing in the presence or absence of ouabain, are subjected to EGFP- and mCherry-directed flow cytometry. HeLa cells only exposed to AAV-HR$^{S1.A1}$ served as a control. (**B**) Quantification of transfection efficiency and selector AAV donor delivery. The transfection efficiency and AAV-HR$^{S1.A1}$ donor delivery were determined by mCherry- and EGFP-directed flow cytometry at 3 days post-transduction (left and central graphs, respectively). The frequencies of transfected and transduced cells are also plotted (right graph). (**C**) Quantification of selector AAV-based DNA editing. The AAV stable transduction levels, serving as a proxy for genome editing frequencies, were determined at 20 days post-transduction by EGFP-directed flow cytometry. The cross indicates complete cell death in ouabain-treated cultures exposed exclusively to AAV-HR$^{S1.A1}$.

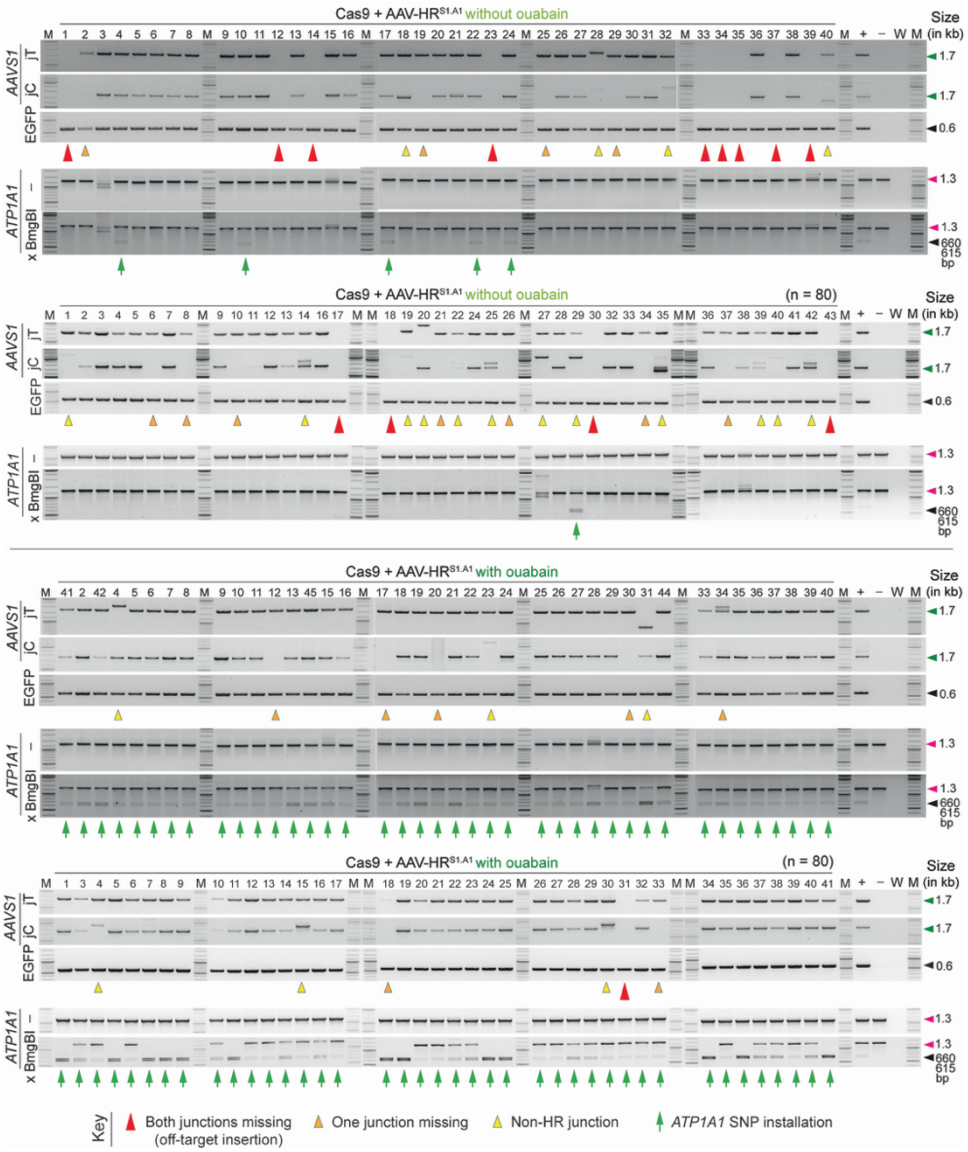

Supplementary Figure S2. Characterization of *AAVS1* and *ATP1A1* co-targeting resulting from selectable AAV donor delivery. PCR genotyping of individual genetically-modified cell clones generated via AAV-HR$^{S1.A1}$ transduction of HeLa cells transfected with a Cas9-encoding plasmid. Prior to clone isolation, the HeLa cell populations were expanded either in the presence or absence of ouabain. Nuclease-free water (W) and DNA from unmodified HeLa cells (-) provided for negative controls; genomic DNA from sorted EGFP-positive HeLa cells exposed to Cas9 and AAV-HR$^{S1.A1}$, served as positive control (+). The *AAVS1* and *ATP1A1* genotype screens involved junction

PCR (jC and jT) and RFLP (×BmgBI) assays, respectively. Clones lacking *AAVS1* targeted insertions or with only one HR-derived junction between transgenic and *AAVS1* sequences are marked by red and orange arrowheads, respectively; whilst clones containing HR-independent donor DNA insertions are highlighted by yellow arrowheads. The remaining clones, modified through precise HR events involving the telomeric and centromeric side of the target sequence (jT and jC, respectively), are not highlighted. Clones with edited *ATP1A1* alleles, scored via BmgBI amplicon digestion, are marked by green arrows. The cumulative datasets corresponding to these *AAVS1* and *ATP1A1* genotype screens (n=160 clones representing independent genome-modifying events), are plotted in **Figure 1F**.

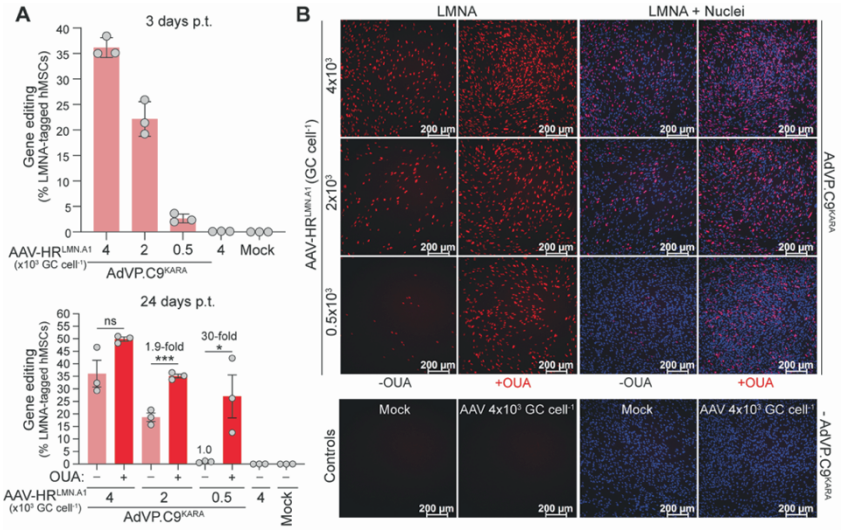

Supplementary Figure S3. Selector AAV gene editing of *LMNA* in hMSCs using combinatorial viral vector delivery. (**A**) Quantification of AAV gene editing with and without ouabain. hMSCs were co-transduced with AAV-HR$^{LMN.A1}$ and AdVP.C9^{KARA} at the specified doses. Gene editing frequencies were measured through mScarlet-directed flow cytometry at 3- and 24- days post-transduction (top and bottom graph, respectively). Prior to flow cytometry analysis at the latter timepoint, the hMSCs were cultured in the presence or absence of ouabain. Mock-transduced hMSCs and hMSCs transduced only with the highest dose of AAV-HR$^{LMN.A1}$ provided for negative controls. The results are presented as mean ± SD of three biological replicates. Significant differences amongst the marked datasets were calculated by Student's t-tests; $^{**}P<0.05$. (**B**) Characterization of LMNA protein tagging in hMSCs. LMNA tagging and nuclear localization was monitored by combining direct fluorescence microscopy for the reporter mScarlet and the DNA dye Hoechst 33342, respectively.

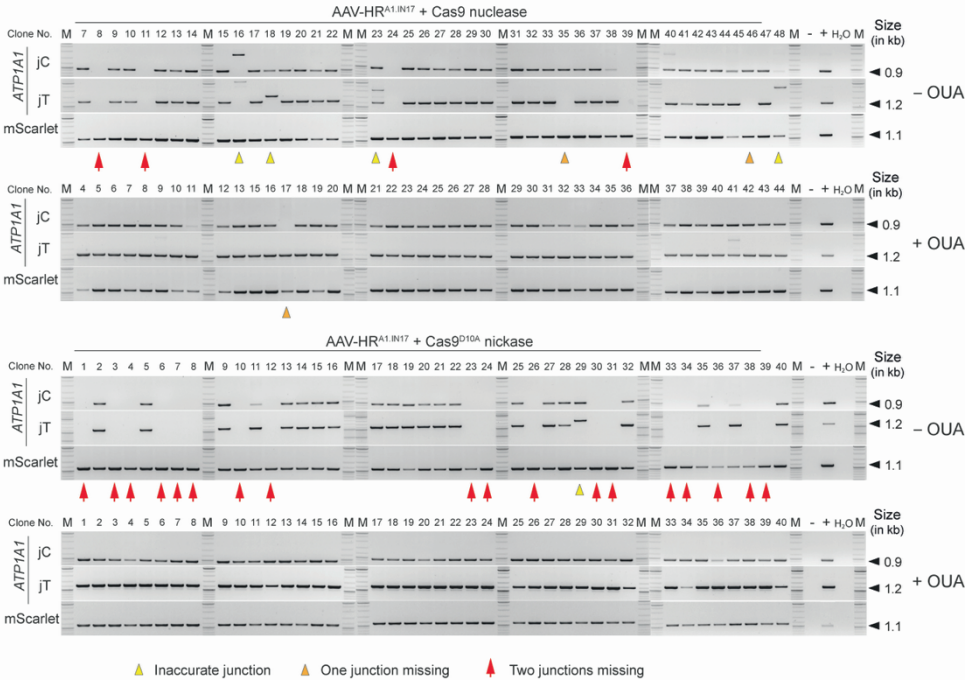

Supplementary Figure S4. Characterization of *ATP1A1* gene targeting resulting from selectable in-linkage AAV donor delivery. PCR genotyping of individual genetically-modified cell clones generated via AAV-HR$^{A1.IN17}$ transduction of HeLa cells transfected with a Cas9- or Cas9^{D10A}-encoding plasmids. Prior to clone isolation, the HeLa cell populations were expanded either in the presence or absence of ouabain. Nuclease-free water (W) and DNA from unmodified HeLa cells (-) provided for negative controls; genomic DNA from sorted mScarlet-positive HeLa cells exposed to Cas9 or Cas9^{D10A} and AAV-HR$^{A1.IN17}$, served as positive controls (+). The *ATP1A1* genotype screens involved junction PCR (jC and jT) analysis. Clones lacking *ATP1A1* targeted insertions or with only one HR-derived junction between transgenic and *ATP1A1* sequences are marked by red and orange arrowheads, respectively; whilst clones containing HR-independent donor DNA insertions are highlighted by yellow arrowheads. The remaining clones, modified through precise HR events involving the telomeric and centromeric side of the target sequence (jT and jC, respectively), are not highlighted. The cumulative datasets corresponding to these *ATP1A1* genotype screens (n=160 clones representing independent genome-modifying events), are plotted in **Figure 4E**.

Supplementary Tables

Supplementary Table S1. Titres of AAV vectors generated for this study.

Plasmid code	**AAV/AdVP vector**	**Titre**
BI17	AAV-HR$^{S1.A1}$	1.86E+08 TU/mL
BI19	AAV-HR$^{LMN.A1}$	1.14E+11 GC/mL
BI38	AAV-HR$^{A1.IN17}$	8.61E+07 TU/mL
U67	AdVP.C9^{KARA}	5.43E+07 GC/mL

Supplementary Table S2. Primers and PCR mixtures used for clonal screening of *AAVS1* (**Figures 1E**, **1F** and **Supplementary figure S2**)

Target	Primer code	Primers (5' → 3') / final concentrations (µM)	2X Phire Tissue Direct PCR Master mix µl	DMSO	Amplicon size (bp)
GFP	#978	GAGCTGGACGGCGACGTAAACG / 0,5	10		596
	#979	CGCTTCTCGTTGGGGTCTTTGCT / 0,5			
jT.*AAVS1*	#986	AACCCCAACCCCGTGGAAG / 0,5	10	2%	1666
	#1004	GCACCGTCCGCTTCGAG / 0,5			
jC.*AAVS1*	#1046	CGACAACCACTACCTGAGCA / 0,5	10		1712
	#1047	GACCTGCCTGGAGAAGGAT / 0,5			

Supplementary Table S3. PCR cycling parameters used for clonal screening of *AAVS1* (**Figures 1E**, **1F** and **Supplementary figure S2**)

Target	Initial denaturation	Denaturation	Annealing	Elongation	Cycles	Final elongation
GFP	98 °C	98 °C	72 °C		35	72 °C
	5 min	5 sec	20 sec			2 min
jT.*AAVS1*	98 °C	98 °C	72 °C		35	72 °C
	5 min	7 sec	30 sec			2 min
jC.*AAVS1*	98 °C	98 °C	72 °C	72 °C	TD 0,5 °C decrease/cycle*10	72 °C
	5 min	7 sec	7 sec	32 sec		
		98 °C	67 °C	72 °C	25	2 min
		7 sec	7 sec	32 sec		

Supplementary Table S4. Primers and PCR mixtures used for clonal screening of *ATP1A1* (**Figures 1E**, **1F** and **Supplementary figure S2**)

Target	Primer code	Primers (5' → 3') / final concentrations (µM)	dNTP (mM)	$MgCl_2$ (mM)	GoTaq Flexi Buffer	GoTaq (Units)	Amplicon size (bp)
ATP1A1	#2225	CCCCTCCCGACAAAATCAATAC/0,4	0.4	1	1x	1.25	1275
	#2228	TAGCACCACACCCAGGTACA/0,4					

Supplementary Table S5. PCR cycling parameters used for clonal screening of *ATP1A1* (**Figures 1E**, **1F** and **Supplementary figure S2**)

Target	Initial denaturation	Denaturation	Annealing	Elongation	Cycles	Final elongation
ATP1A1	95 ℃	95 ℃	64 ℃	72 ℃	40	72 ℃
	5 min	30 sec	30 sec	1 min 20 sec		5 min

Supplementary Table S6. Primers and PCR mixtures used for genotyping of *AAVS1* and *ATP1A1* (**Figures 2D**)

Target	Primer code	Primers (5' → 3') / final concentrations (μM)	dNTP (mM)	$MgCl_2$ (mM)	GoTaq Flexi Buffer	GoTaq (Units)	DMSO	Amplicon size (bp)
EGFP	#978	GAGCTGGACGGCGACGTAAACG / 0,4	0.4	1	1×	1.25		596
	#979	CGCTTCTCGTTGGGGTCTTTGCT / 0,4						
jT.*AAVS1*	#986	AACCCCAACCCCGTGGAAG / 0,4	0.4	1	1×	1.25	2%	1666
	#1004	GCACCGTCCGCTTCGAG / 0,4						
jC.*AAVS1*	#1046	CGACAACCACTACCTGAGCA / 0,4	0.4	1	1×	1.25		1712
	#1047	GACCTGCCTGGAGAAGGAT / 0,4						
ATP1A1	#2225	CCCCTCCCGACAAAATCAATAC / 0.4	0.4	1	1×	1.25		1275
	#2228	TAGCACCACACCCAGGTACA / 0.4						

Supplementary Table S7. PCR cycling parameters used for genotyping of *AAVS1* and *ATP1A1* (**Figures 2D**)

Target	Initial denaturation	Denaturation	Annealing	Elongation	Cycles	Final elongation
EGFP	95 ℃	95 ℃	72 ℃		35	72 ℃
	5 min	30 sec	20 sec			5 min
jT.*AAVS1*	95 ℃	95 ℃	61 ℃	72 ℃	35	72 ℃
	5 min	30 sec	30 sec	1 min 30 sec		1 min 30 sec
jC.*AAVS1*	95 ℃	95 ℃	67 ℃	72 ℃	35	72 ℃
	5 min	30 sec	30 sec	1 min 30 sec		1 min 30 sec
ATP1A1	95 ℃	95 ℃	64 ℃	72 ℃	40	72 ℃
	5 min	30 sec	30 sec	1 min 20 sec		5 min

Supplementary Table S8. Primers and PCR mixtures used for genotyping of *LMNA* and *ATP1A1* (**Figures 3C**, **3E**)

Target	Primer code	Primers (5' → 3') / final concentrations (μM)	dNTP (mM)	$MgCl_2$ (mM)	GoTaq Flexi Buffer	GoTaq (Units)	Amplicon size (bp)
mScarlet	#2328	CACGAGTTCGAGATCGAGGG / 0.4	0.2	1	1x	1.25	573
	#2329	TTCGTACTGTTCCACCACGG / 0.4					
jT.*LMNA*	#2332	GAACAGTACGAACGCTCCGA / 0.4	0.2	1	1x	1.25	781
	#2333	CTGGGTGCCCAGAGTTCTTC / 0.4					
jC.*LMNA*	#2330	TGAGTCACACTGATGGGCAC / 0.4	0.2	1	1x	1.25	1263
	#2331	GGTGTAGTCCTCGTTGTGGG / 0.4					
ATP1A1	#2225	CCCCTCCCGACAAAATCAATAC / 0.4	0.2	1	1x	1.25	1275
	#2228	TAGCACCACACCCAGGTACA / 0.4					

Supplementary Table S9. PCR cycling parameters used genotyping of *LMNA* and *ATP1A1* (**Figures 3C**, **3E**)

Target	Initial denaturation	Denaturation	Annealing	Elongation	Cycles	Final elongation
mScarlet	95 ℃	95 ℃	62.9 ℃	72 ℃	30	72 ℃
	5 min	30 sec	30 sec	30 sec		5 min
jT.*LMNA*	95 ℃	95 ℃	62.9 ℃	72 ℃	30	72 ℃
	5 min	30 sec	30 sec	40 sec		5 min
jC.*LMNA*	95 ℃	95 ℃	62.9 ℃	72 ℃	30	72 ℃
	5 min	30 sec	30 sec	1 min		5 min
ATP1A1	95 ℃	95 ℃	64 ℃	72 ℃	30	72 ℃
	5 min	30 sec	30 sec	1 min		5 min

Supplementary Table S10. Primers and PCR mixtures used for clonal screening of *ATP1A1::mScarlet* (**Figures 4E** and **Supplementary figure S4**)

Target	Primer code	Primers (5' → 3') / final concentrations (µM)	2X Phire Tissue Direct PCR Master mix µl	Amplicon size (bp)
mScarlet	#2120	ACGGTGTAGTCCTCGTTGTG / 0.5	10	1095
	#1648	TCTCGCACATTCTTCACGTC / 0.5		
jT.*ATP1A1*	#2229	ACTACAGGGCGTGCATACAG / 0.5	10	1199
	#2230	CCCACAACGAGGACTACACC / 0.5		
jC.*ATP1A1*	#2234	GGTGACCTACCAGCCAAACT / 0.5	10	945
	#2235	CTTGGAAAAGGCGCAACCC / 0.5		

Supplementary Table S11. PCR cycling parameters used for clonal screening of *ATP1A1::mScarlet* (**Figures 4E** and **Supplementary figure S4**)

Target	Initial denaturation	Denaturation	Annealing	Elongation	Cycles	Final elongation
mScarlet	98 °C	98 °C	72 °C		30	72 °C
	5 min	7 sec	32 sec			2 min
jT.*ATP1A1*	98 °C	98 °C	67 °C	72 °C	30	72 °C
	5 min	7 sec	5 sec	20 sec		2 min
jC.*ATP1A1*	98 °C	98 °C	72 °C		35	72 °C
	5 min	7 sec	20 sec			2 min

Supplementary Table S12. Primers and PCR mixtures used for junction PCR analysis of *ATP1A1::mScarlet* (**Figures 5F**)

Target	Primer code	Primers (5' → 3') / final concentrations (μM)	dNTP (mM)	$MgCl_2$ (mM)	GoTaq Flexi Buffer	GoTaq (Units)	Amplicon size (bp)
mScarlet	#2120	ACGGTGTAGTCCTCGTTGTG / 0.4	0.4	1	1x	1.25	1095
	#1648	TCTCGCACATTCTTCACGTC / 0.4					
jT.*ATP1A1*	#2229	ACTACAGGGCGTGCATACAG / 0.4	0.4	1	1x	1.25	1199
	#2230	CCCACAACGAGGACTACACC / 0.4					
jC.*ATP1A1*	#2234	GGTGACCTACCAGCCAAACT / 0.4	0.4	1	1x	1.25	945
	#2235	CTTGGAAAAGGCGCAACCC / 0.4					

Supplementary Table S13. PCR cycling parameters used for junction PCR analysis of *ATP1A1::mScarlet* (**Figures 5F**)

Target	Initial denaturation	Denaturation	Annealing	Elongation	Cycles	Final elongation
mScarlet	95 ℃	95 ℃	63 ℃	72 ℃	35	72 ℃
	5 min	30 sec	30 sec	1 min		5 min
jT.*ATP1A1*	95 ℃	95 ℃	65 ℃	72 ℃	35	72 ℃
	5 min	30 sec	30 sec	1 min		1 min 30 sec
jC.*ATP1A1*	95 ℃	95 ℃	65 ℃	72 ℃	35	72 ℃
	5 min	30 sec	30 sec	1 min		1 min 30 sec

Supplementary Information

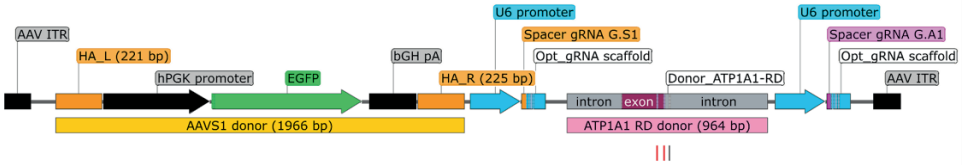

>BI17_pAAV-HR$^{S1.A1}$ (4304 bp)

ctggcgcgctcgctcgctcactgaggccgcccgggcaaagcccgggcgtcgggcgacctttggtcgcccggcct
cagtgagcgagcgagcgcgcagagagggagtggccaactccatcactaggggttccttgtagttaatgattaac
ccgccatgctacttatctacgtggccactagtacttctcgagctctgtacatgtccgcggtcgcgacgtacgcg
tatcgatggcgccagctgcagagctctagctcttccagccccctgtcatggcatcttccaggggtccgagagct
cagctagtcttcttcctccaacccgggcccctatgtccacttcaggacagcatgtttgctgcctccagggatcc
tgtgtccccgagctgggaccaccttatattcccagggccggttaatgtggctctggttctgggtacttttatct
gtcccctccaccccacagtggggcaagcttccacggggttggggttgcgccttttccaaggcagccctgggttt
gcgcagggacgcggctgctctgggcgtggttccgggaaacgcagcggcgccgaccctgggtctcgcacattctt
cacgtccgttcgcagcgtcacccggatcttcgccgctacccttgtgggccccccgggcgacgcttcctgctccgc
ccctaagtcgggaaggttccttgcggttcgcggcgtgccggacgtgacaaacggaagccgcacgtctcactagt
accctcgcagacggacagcgccagggagcaatggcagcgcgccgaccgcgatgggctgtggccaatagcggctg
ctcagcagggcgcgccgagagcagcggccgggaaggggcggtgcgggaggcggggtgtggggcggtagtgtggg
ccctgttcctgcccgcgcggtgttccgcattctgcaagcctccggagcgcacgtcggcagtcggctccctcgtt
gaccgaatcaccgacctctctccccaccggtcgccaccatggtgagcaagggcgaggagctgttcaccggggtg
gtgcccatcctggtcgagctggacggcgacgtaaacggccacaagttcagcgtgtccggcgagggcgagggcga
tgccacctacggcaagctgaccctgaagttcatctgcaccaccggcaagctgcccgtgccctggcccaccctcg
tgaccaccctgacctacggcgtgcagtgcttcagccgctaccccgaccacatgaagcagcacgacttcttcaag
tccgccatgcccgaaggctacgtccaggagcgcaccatcttcttcaaggacgacggcaactacaagacccgcgc
cgaggtgaagttcgagggcgacaccctggtgaaccgcatcgagctgaagggcatcgacttcaaggaggacggca
acatcctggggcacaagctggagtacaactacaacagccacaacgtctatatcatggccgacaagcagaagaac
ggcatcaaggtgaacttcaagatccgccacaacatcgaggacggcagcgtgcagctcgccgaccactaccagca
gaacaccccatcggcgacggccccgtgctgctgcccgacaaccactacctgagcacccagtccgccctgagca
aagaccccaacgagaagcgcgatcacatggtcctgctggagttcgtgaccgccgccgggatcactctcggcatg
gacgagctgtacaagtaaagcggccggccgcgtcgagtctaggatcagcctcgactgtgccttctagttgccag
ccatctgttgtttgcccctcccccgtgccttccttgaccctggaaggtgccactcccactgtcctttcctaata
aaatgaggaaattgcatcgcattgtctgagtaggtgtcattctattctgggggggtggggtggggcaggacagca
agggggaggattgggaagacaatagcaggcatgctggggatgcggtgggctctatggaagcttactagggaca
ggattggtgacagaaaagccccatccttaggcctcctccttcctagtctcctgatattgggtctaaccccccacc
tcctgttaggcagattccttatctggtgacacacccccatttcctggagccatctctctccttgccagaacctc
taaggtttgcttacgatggagccagagaggatcctgggagggagagcttggcaggggggtgggagggagctagag
tccggccgcccccttcaccgagggcctatttcccatgattccttcatatttgcatatacgatacaaggctgtta
gagagataattggaattaatttgactgtaaacacaaagatattagtacaaaatacgtgacgtagaaagtaataa
tttcttgggtagtttgcagttttaaaattatgttttaaaatggactatcatatgcttaccgtaacttgaaagta
tttcgatttcttggctttatatatcttgtggaaaggacgaaacaccggggccactagggacaggatgtttcaga
gctatgctggaaacagcatagcaagttgaaataaggctagtccgttatcaacttgaaaaagtggcaccgagtcg
gtgctttttttgaattcactggccgtcgttttacaacgtcgtgactgggaaaaccctggcgttacccaacttaa
tcgccttgcagcacatccccctttcgccagaacaaccggtacaaatttattgatggatcaatttaaagagttt
taatctgggtgttatgagttccttgggcctattgtttgcctgaaccctgtggggactggctcatcagcagaatt
attcatggaggaatttgctaggttttaccttggctctctagcttgggacattttgtttcttccttaaatcctta
ttgcaaccgtccagctaccaggtaggtatattgccttgtaagtgctggtacagtttgccttatttatattccac
tgcttctcagggattaacatctgctcgtgcagctgagatcctggcgcgagatggtcccaacgccctcactcccc
ctcccactactcctgaatggatcaagttttgtcggcagctctttgggggttctcaatgttactgtggattgga
gcgattctttgtttcttggcttatagcatcagagctgctacagaagaggaacctcaaaacgatgacgtgagttc

tgtaattcagcatatcgatttgtagtacacatcagatatcttctccgtctttgtctcccacttcttctcaatta
ccactcattacttaatggttatgaactcattacttaatggttatgaacagctgttgccttcaaggctcatccat
tcttccttcgtttccatttcctctctctaccacccacgttgtagatgctcttacaagtgggatgcccacctgca
tgtgctgctgtgagcaggcagctctgctcaggccccggccgccacccactggatggcagagcacagcgattcat
gttggcacatccacctgtccagaaatgcttggtggccattcttcaaaatccacaagttggttgaaaaacaatct
ttgttttataaagcaggagaaactgatgcatctagaacctttccaaacgtccagttagtgatcaagtgttggtg
tgcctgactccatttctgacccttcctgtgtggtctttagaaggGAATTGGATCCTAGAGTCCGGCCGCCCCCT
TCACCgagggcctatttcccatgattccttcatatttgcatatacgatacaaggctgttagagagataattgga
attaatttgactgtaaacacaaagatattagtacaaaatacgtgacgtagaaagtaataatttcttgggtagtt
tgcagttttaaaattatgttttaaaatggactatcatatgcttaccgtaacttgaaagtatttcgatttcttgg
ctttatatatcttgtggaaaggacgaaacaccgagttctgtaattcagcatagtttcagagctatgctggaaac
agcatagcaagttgaaataaggctagtccgttatcaacttgaaaaagtggcaccgagtcggtgcttttttgaa
ttgatccatatatagggcccgggttataattacctcaggtcgacgtcccatgtgcaggtgctgaattgtagata
agtagcatggcgggttaatcattaactacaaggaacccctagtgatggagttggccactccctctctgcgcgct
cgctcgctcactgaggccgggcgaccaaaggtcgcccgacgcccgggctttgcccgggcggcctcagtgagcga
gcgagcgcgcag

Map and nucleotide sequence of selector AAV donor construct BI17_pAAV-HR$^{S1.A1}$. Diagram of AAV-HR$^{S1.A1}$ vector genome containing an *AAVS1*-targeting HR donor template (1966 bp). The selector donor DNA sequence (964 bp) is designed for installing the ouabain resistance gain-of-function Q118R and N129D SNPs (RD), vertical red dashes, within the exon 4 of *ATP1A1* upon gRNA G^{A1}-directed cleavage within intron 4. AAV ITR, adeno-associated virus type-2 inverted terminal repeat; orange bars, homology arms ("Left" and "Right") consisting of DNA homologous to sequences flanking the *AAVS1* target site of gRNA G^{S1}; hPGK, human phosphoglycerate kinase 1 gene promoter; EGFP, enhanced green fluorescence protein reporter; bGH pA, bovine growth hormone gene polyadenylation signal; U6 promoter, human U6 snRNA polymerase III promoter driving the expression of each gRNA. The vector plasmid backbone is not shown.

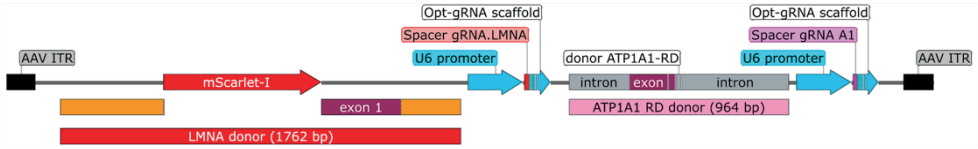

>BI19_pAAV-HR$^{LMN.A1}$ (4075 bp)

ctggcgcgctcgctcgctcactgaggccgcccgggcaaagcccgggcgtcgggcgacctttggtcgcccggcct
cagtgagcgagcgagcgcgcagagagggagtggccaactccatcactaggggttccttgtagttaatgattaac
ccgccatgctacttatctacgtggccactagtacttctcgagctctgtacatgtccgcggtcgatcgcatgcct
gcagagctctagtaccggcaagcttggagccgacagtgctgagcaggcaggagccaagagaggggaagcttgag
cctcacgcagttaggggtgcgctggagagggtggggcccgactccgccacaccccaacggtccttccccctcct
caccactcccgccccacccccaatggatctgggactgccccttaagagtagtggccccctcctcccttcagag
gaggacctattagagcctttgccccggcgtcggtgactcagtgttcgcgggagcgccgcacctacaccagccaa
cccagatcccgaggtccgacagcgcccggcccagatccccacgcctgccaggagcaagccgagagccagccggc
cggcgcactccgactccgagcagtctctgtccttcgacccgagccccgcgccctttccgggacccctgccccgc
gggcagcgctgccaacctgccggccatggtgagcaagggcgaggcagtgatcaaggagttcatgcggttcaagg
tgcacatggagggctccatgaacggccacgagttcgagatcgagggcgagggcgagggccgccctacgagggc
acccagaccgccaagctgaaggtgaccaagggtggcccctgcccttctcctgcccacatcctgtcccctcagtt
catgtacggctccagggccttcatcaagcaccccgccgacatccccgactactataagcagtccttccccgagg
gcttcaagtgggagcgcgtgatgaacttcgaggacggcggcgccgtgaccgtgacccaggacacctccctggag
gacggcaccctgatctacaaggtgaagctccgcggcaccaacttccctcctgacggccccgtaatgcagaagaa
gacaatgggctgggaagcatccaccgagcggttgtaccccgaggacggcgtgctgaagggcgacattaagatgg
ccctgcgcctgaaggacggcggccgctacctggcggacttcaagaccacctacaaggccaagaagcccgtgcag
atgcccggcgcctacaacgtcgaccgcaagttggacatcacctcccacaacgaggactacaccgtggtggaaca
gtacgaacgctccgagggccgccactccaccggcggcatggacgagctgtacaagaccccgtcccagcggcgcg
ccacccgcagcggggcgcaggccagctccactccgctgtcgcccacccgcatcacccggctgcaggagaaggag
gacctgcaggagctcaatgatcgcttggcggtctacatcgaccgtgtgcgctcgctggaaacggagaacgcagg
gctgcgccttcgcatcaccgagtctgaagaggtggtcagccgcgaggtgtccggcatcaaggccgcctacgagg
ccgagctcggggatgcccgcaagacccttgactcagtagccaaggagcgcgcccgcctgcagctggagctgagc
aaagtgcgtgaggagtttaaggagctgaaagcgcggtgagttcgcccaggtggctgcgtgcctggcggggagtg
gagagggcggcgggccggcgcccctggccggccgcaggaagggagtgagagggcctggaggccgataactttgc
catagtctcctcccctccccggaactgccccagcgggtgactggcagtgtcaaggggaattgtcaagacaggac
agagagggaagtggtggtctctgggagagggtcggggaggatataaggaatggtgggggtatcagggacaagtt
ggcgaattctagagtccggccgccccttcaccgagggcctatttcccatgattccttcatatttgcatatacg
atacaaggctgttagagagataattggaattaatttgactgtaaacacaaagatattagtacaaaatacgtgac
gtagaaagtaataatttcttgggtagtttgcagttttaaaattatgttttaaaatggactatcatatgcttacc
gtaacttgaaagtatttcgatttcttggctttatatatcttgtggaaaggacgaaacaccgccatggagacccc
gtcccaggtttcagagctatgctggaaacagcatagcaagttgaaataaggctagtccgttatcaacttgaaaa
agtggcaccgagtcggtgctttttttgaattcggtaccggcgcgcccgtacgactaggcctattaatattccgg
agtatacgtagccggctaacgttaacaaccggtacaaatttattgatggatcaatttaaagagttttaatctg
ggtgttatgagttccttgggcctattgtttgcctgaaccctgtggggactggctcatcagcagaattattcatg
gaggaatttgctaggttttaccttggctctctagcttgggacattttgtttcttccttaaatccttattgcaac
cgtccagctaccaggtaggtatattgccttgtaagtgctggtacagtttgccttatttatattccactgcttct
cagggattaacatctgctcgtgcagctgagatcctggcgcgagatggtcccaacgccctcactccccctcccac
tactcctgaatggatcaagttttgtcggcagctctttgggggttctcaatgttactgtggattggagcgattc
tttgtttcttggcttatagcatcagagctgctacagaagaggaacctcaaaacgatgacgtgagttctgtaatt
cagcatatcgatttgtagtacacatcagatatcttctccgtctttgtctcccacttcttctcaattaccactca
ttacttaatggttatgaactcattacttaatggttatgaacagctgttgccttcaaggctcatccattcttcct
tcgtttccatttcctctctctaccacccacgttgtagatgctcttacaagtgggatgcccacctgcatgtgctg
ctgtgagcaggcagctctgctcaggccccggccgccacccactggatggcagagcacagcgattcatgttggca
catccacctgtccagaaatgcttggtggccattcttcaaaatccacaagttggttgaaaaacaatctttgtttt
ataaagcaggagaaactgatgcatctagaacctttccaaacgtccagttagtgatcaagtgttggtgtgcctga

ctccatttctgacccttcctgtgtggtctttagaaggGAATTGGATCCTAGAGTCCGGCCGCCCCCTTCACCga
gggcctatttcccatgattccttcatatttgcatatacgatacaaggctgttagagagataattggaattaatt
tgactgtaaacacaaagatattagtacaaaatacgtgacgtagaaagtaataatttcttgggtagtttgcagtt
ttaaaattatgttttaaaatggactatcatatgcttaccgtaacttgaaagtatttcgatttcttggctttata
tatcttgtggaaaggacgaaacaccgagttctgtaattcagcatagtttcagagctatgctggaaacagcatag
caagttgaaataaggctagtccgttatcaacttgaaaaagtggcaccgagtcggtgctttttttgaattgatcc
atatatagggcccgggttataattacctcaggtcgacgtcccatgtgcaggtgctgaattgtagataagtagca
tggcgggttaatcattaactacaaggaacccctagtgatggagttggccactccctctctgcgcgctcgctcgc
tcactgaggccgggcgaccaaaggtcgcccgacgcccgggctttgcccgggcggcctcagtgagcgagcgagcg
cgcag

Map and nucleotide sequence of selector AAV donor construct BI19_pAAV-HR$^{LMN.A1}$. Diagram of AAV-HR$^{LMN.A1}$ vector genome containing an *LMNA*-targeting HR donor template (1762 bp). The selector donor DNA sequence (964 bp) is designed for installing the ouabain resistance gain-of-function Q118R and N129D SNPs (RD) within the exon 4 of *ATP1A1* upon gRNA G^{A1}-directed cleavage within intron 4. AAV ITR, adeno-associated virus type-2 inverted terminal repeat; DNA sequences homologous to target *LMNA* alleles (homology arms) flank the mScarlet-1 reporter coding sequence (red arrow). The gRNA^{LMNA} directs HR-mediated *LMNA* gene tagging upon targeted DNA cleavage at the N-terminus of *LMNA* alleles. U6 promoter, human U6 snRNA polymerase III promoter driving the expression of each gRNA. The vector plasmid backbone is not shown.

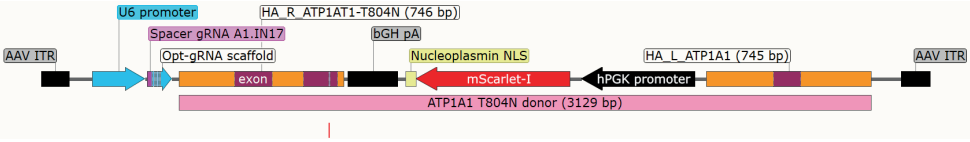

>BI38_pAAV-HR$^{A1.IN17}$ (4014 bp)

ctggcgcgctcgctcgctcactgaggccgcccgggcaaagcccgggcgtcgggcgacctttggtcgcccggcc
tcagtgagcgagcgagcgcgcagagagggagtggccaactccatcactaggggttccttgtagttaatgatta
acccgccatgctacttatctacgtggccactagtacttctcgagctctacgtagaattctctagagtccggcc
gccccttcaccgagggcctatttcccatgattccttcatatttgcatatacgatacaaggctgttagagaga
taattggaattaatttgactgtaaacacaaagatattagtacaaaatacgtgacgtagaaagtaataatttct
tgggtagtttgcagttttaaaattatgttttaaaatggactatcatatgcttaccgtaacttgaaagtatttc
gatttcttggctttatatatcttgtggaaaggacgaaacaccgtcacagatcgatagtagtggtttcagagct
atgctggaaacagcatagcaagttgaaataaggctagtccgttatcaacttgaaaaagtggcaccgagtcggt
gctttttttgaattcggtacgagcgctgctaggcaattccacccaccagagtcattactttgagtagctcttg
ttaatgctgggggctatgtttgttgtcacttctcagttctgttatttggtgtagggcctgtgtgaatacttgc
ctgtgacggttctcaggcttcataaatagtctcaataggaaaggagcagtgtctgtaatgagtgctcagtggg
ggcatgcatcgcactatttccatcgctaggaaaagtgattggtattaacccgttttccctttctggggtagg
gtgctatcgtggctgtgactggtgacggtgtgaatgactctccagctttgaagaaagcagacattggggttgc
tatggggattgctggctcagatgtgtccaagcaagctgctgacatgattcttctggatgacaactttgcctca
attgtgactggagtagaggaaggtgagagctatttaaggtgtacaccaagatcttattcagatactgcccatt
agcatccatttctgtatacttcttggatatgttcagtttccagtgtgcttgtctcataagctaacagtaaaaa
atcttggttttcatagtcgtctgatctttgataacttgaagaaatccattgcttataccttaaccagtaaca
ttcccgagatcaccccgttcctgatatttattattgcaaacattccactaccactgggggaatgtcaccatcct
ctgcattgacttgggcactgacatggtgagtgtcacaacagtcacagatcgatatcagacgtgatatgtcgac
ccatagagcccaccgcatccccagcatgcctgctattgtcttcccaatcctcccccttgctgtcctgccccac
cccaccccccagaatagaatgacacctactcagacaatgcgatgcaatttcctcattttattaggaaaggaca
gtgggagtggcaccttccagggtcaaggaaggcacgggggaggggcaaacaacagatggctggcaactagaag
gcacagcctgcagggtttaaacgcggccgctcgagttatcactttttctttttttgcctggccggccttttcg
tggccgccggccttttcttgtacagctcgtccatgccgccggtggagtggcggccctcggagcgttcgtactg
ttccaccacggtgtagtcctcgttgtgggaggtgatgtccaacttgcggtcgacgttgtaggcgccgggcatc
tgcacgggcttcttggccttgtaggtggtcttgaagtccgccaggtagcggccgccgtccttcaggcgcaggg
ccatcttaatgtcgcccttcagcacgccgtcctcggggtacaaccgctcggtggatgcttcccagcccattgt
cttcttctgcattacggggccgtcaggagggaagttggtgccgcggagcttcaccttgtagatcagggtgccg
tcctccagggaggtgtcctgggtcacggtcacggcgccgccgtcctcgaagttcatcacgcgctcccacttga
agccctcgggggaaggactgcttatagtagtcggggatgtcggcggggtgcttgatgaaggccctggagccgta
catgaactgaggggacaggatgtcccaggagaagggcaggggggccacccttggtcaccttcagcttggcggtc
tgggtgccctcgtaggggcggccctcgcccctcgccctcgatctcgaactcgtggccgttcatggagccctcca
tgtgcaccttgaaccgcatgaactccttgatcactgcctcgcccttgctcaccatggctccctgaaaatacag
attctcggcggccgccttaaggctgagggtacccctggggagagaggtcggtgattcggtcaacgagggagcc
gactgccgacgtgcgctccggaggcttgcagaatgcggaacaccgcgcgggcaggaacagggcccacactacc
gccccacaccccgcctcccgcaccgccccttcccggccgctgctctcggcgcgccctgctgagcagccgctat
tggccacagcccatcgcggtcggcgcgctgccattgctccctggcgctgtccgtctgcgagggtactagtgag
acgtgcggcttccgtttgtcacgtccggcacgccgcgaaccgcaaggaaccttcccgacttaggggcggagca
ggaagcgtcgccgggggcccacaagggtagcggcgaagatccgggtgacgctgcgaacggacgtgaagaatg
tgcgagacccagggtcggcgccgctgcgtttcccggaaccacgcccagagcagccgcgtccctgcgcaaaccc
agggctgccttggaaaaggcgcaaccccaaccccgtggatgcattaaaaaacctcccacacctccccctgaac
ctgaaacaagcttgtgaggtgtgagctgtgtcttcattcactggcactatgctcccagcatccatgaggctgg

cgttgggaaaagaaattctcaggaccagtatccagtgtgtgtcccaatcccggcttcacagaatcagtattac
cactcttcaaggcagcagttaacatttgtttatcagatgggaatctttatttttgtatacttcacctaaaaga
tttttaaatgggagggcaagaatttttataacaaaaggttcacaatattagcttccttatttttagtaactaaa
ttccttctccccacccctttcccagGTTCCTGCCATCTCCCTGGCTTATGAGCAGGCTGAGAGTGACATCATGA
agagacagcccagaaatcccaaaacagacaaacttgtgaatgagcggctgatcagcatggcctatgggcagat
tggtaagctgcagcctggagtgggaagctggcacatctaaggcatctgaggtgatggtgtccacctcaggttg
aggttgatttcagagactgcaaatccaggcgactttcaggtctaggatgagccctaacggagtgagcctgtgg
agtttctctgaactctcttccatgtgagaatacatctgttgctgtttgcccagttacctttttgtggaaactgg
ttttctatactgagcaccttggaactgggctcaactctgcctgagaaatgaggatgtccttcctcactgagcc
ttgcggaacaggaggcatggttctaaggGCTAGTCCTAGCCACGTGACCGGTTCGCGAGGATCCATATATAGG
gcccgggttataattacctcaggtcgacgtcccatgtgcaggtgctgaattgtagataagtagcatggcgggt
taatcattaactacaaggaACCCCTAGTGATGGAGTTGGCCACTCCCTCTCTGCGCGCTCGCTCGCTCACTGA
GGCCGGGCGACCAAAGGTCGCCCGACGCCCGGGCTTTGCCCGGGCGGCCTCAGTGAGCGAGCGAGCGCGCAG

Map and nucleotide sequence of selector AAV donor construct BI38_pAAV-HR$^{A1.IN17}$. Diagram of AAV-HR$^{A1.IN17}$ vector genome containing an *ATP1A1*-targeting HR donor template. The selector donor DNA sequence (3129 bp bp) is designed for concomitant HR-mediated installation of a transgene and an ouabain resistance gain-of-function SPN (T804N) within exon 17 and intron 17 of *ATP1A1* alleles, respectively. The matched gRNA G$^{A1.IN17}$ directs DNA cleavage at the ATP1A1 intron 17. U6 promoter, human U6 snRNA polymerase III promoter driving the expression of gRNA$^{A1.IN17}$ AAV ITR, adeno-associated virus type-2 inverted terminal repeat; DNA sequences homologous to target *ATP1A1* alleles (homology arms) flank a transgene consisting of the human phosphoglycerate kinase 1 gene promoter (hPGK); the mScarlet-1 reporter coding sequence (red arrow), and the bovine growth hormone gene polyadenylation signal (bGH pA). The vector plasmid backbone is not shown.

References

1. Pacesa M, Pelea O, Jinek M. Past, present, and future of CRISPR genome editing technologies. Cell 2024 187:1076-1100.
2. Hongyu Liao, Jiahao Wu, Nathan J. VanDusen, Yifei Li, Yanjiang Zheng CRISPR/Cas9-mediated homology-directed repair for precise gene editing. Mol Ther Nucleic Acids 2024 DOI: 10.1016/j.omtn.2024.102344.
3. He X., Tan C., Wang F., Wang Y., Zhou R., Cui D., You W., Zhao H., Ren J., Feng B. Knockin of large reporter genes in human cells via CRISPR/Cas9-induced homology-dependent and independent DNA repair. Nucleic Acids Res. 2016; 44:e85.
4. Suzuki K, Tsunekawa Y, Hernandez-Benitez R, Wu J, Zhu J, Kim EJ, Hatanaka F, Yamamoto M, Araoka T, Li Z, Kurita M, Hishida T, Li M, Aizawa E, Guo S, Chen S, Goebl A, Soligalla RD, Qu J, Jiang T, Fu X, Jafari M, Esteban CR, Berggren WT, Lajara J, Nuñez-Delicado E, Guillen P, Campistol JM, Matsuzaki F, Liu GH, Magistretti P,

Zhang K, Callaway EM, Zhang K, Belmonte JC. In vivo genome editing via CRISPR/Cas9 mediated homology-independent targeted integration. Nature 2016 540:144-149.

5. Bischoff N, Wimberger S, Maresca M, Brakebusch C. Improving Precise CRISPR Genome Editing by Small Molecules: Is there a Magic Potion? Cells 2020 9:1318.
6. Chu VT, Weber T, Wefers B, Wurst W, Sander S, Rajewsky K, Kühn R. Increasing the efficiency of homology-directed repair for CRISPR-Cas9-induced precise gene editing in mammalian cells. Nat. Biotechnol. 2015 33:543-548.
7. Wimberger S, Akrap N, Firth M, Brengdahl J, Engberg S, Schwinn MK, Slater MR, Lundin A, Hsieh PP, Li S, Cerboni S, Sumner J, Bestas B, Schiffthaler B, Magnusson B, Di Castro S, Iyer P, Bohlooly-Y M, Machleidt T, Rees S, Engkvist O, Norris T, Cadogan EB, Forment JV, Šviković S, Akcakaya P, Taheri-Ghahfarokhi A, Maresca M. Simultaneous inhibition of DNA-PK and PolΘ improves integration efficiency and precision of genome editing. Nat. Commun. 2023 14:4761.
8. Schimmel J, Muñoz-Subirana N, Kool H, van Schendel R, van der Vlies S, Kamp JA, de Vrij FMS, Kushner SA, Smith GCM, Boulton SJ, Tijsterman M. Modulating mutational outcomes and improving precise gene editing at CRISPR-Cas9-induced breaks by chemical inhibition of end-joining pathways. Cell Rep. 2023 42:112019.
9. Mikkelsen NS, Bak RO. Enrichment strategies to enhance genome editing. J Biomed Sci. 2023 30:51.
10. Shy BR, MacDougall MS, Clarke R, Merrill BJ. Co-incident insertion enables high efficiency genome engineering in mouse embryonic stem cells. Nucleic Acids Res. 2016 44:7997-8010.
11. Mitzelfelt KA, McDermott-Roe C, Grzybowski MN, Marquez M, Kuo CT, Riedel M, Lai S, Choi MJ, Kolander KD, Helbling D, Dimmock DP, Battle MA, Jou CJ, Tristani-Firouzi M, Verbsky JW, Benjamin IJ, Geurts AM. Efficient Precision Genome Editing in iPSCs via Genetic Co-targeting with Selection. Stem Cell Reports 2017 8:491-499.
12. Agudelo D, Duringer A, Bozoyan L, Huard CC, Carter S, Loehr J, Synodinou D, Drouin M, Salsman J, Dellaire G, Laganière J, Doyon Y. Marker-free coselection for CRISPR-driven genome editing in human cells. Nat Methods 2017 14:615-620.
13. Wiebking V, Patterson JO, Martin R, Chanda MK, Lee CM, Srifa W, Bao G, Porteus MH. Metabolic engineering generates a transgene-free safety switch for cell therapy. Nat. Biotechnol. 2020 38:1441-1450.
14. Li S, Akrap N, Cerboni S, Porritt MJ, Wimberger S, Lundin A, Möller C, Firth M, Gordon E, Lazovic B, Sieńska A, Pane LS, Coelho MA, Ciotta G, Pellegrini G, Sini M, Xu X, Mitra S, Bohlooly-Y M, Taylor BJM, Sienski G, Maresca M. Universal toxin-

based selection for precise genome engineering in human cells. Nat Commun. 2021 12:497.

15. Wu J, Li D, Du L, Baldawi M, Gable ME, Askari A, Liu L. Ouabain prevents pathological cardiac hypertrophy and heart failure through activation of phosphoinositide 3-kinase α in mouse. Cell Biosci. 2015 5:64.
16. Levesque S, Mayorga D, Fiset JP, Goupil C, Duringer A, Loiselle A, Bouchard E, Agudelo D, Doyon Y. Marker-free co-selection for successive rounds of prime editing in human cells. Nat Commun. 2022 13:5909.
17. Epstein BE, Schaffer DV. Combining Engineered Nucleases with Adeno-associated Viral Vectors for Therapeutic Gene Editing. Adv Exp Med Biol. 2017;1016:29-42.
18. Miller DG, Petek LM, Russell DW. Adeno-associated virus vectors integrate at chromosome breakage sites. Nat Genet. 2004 36:767-773.
19. Hanlon KS, Kleinstiver BP, Garcia SP, Zaborowski MP, Volak A, Spirig SE, Muller A, Sousa AA, Tsai SQ, Bengtsson NE, Lööv C, Ingelsson M, Chamberlain JS, Corey DP, Aryee MJ, Joung JK, Breakefield XO, Maguire CA, György B. High levels of AAV vector integration into CRISPR-induced DNA breaks. Nat Commun. 2019 10:4439.
20. Ferrari S, Jacob A, Cesana D, Laugel M, Beretta S, Varesi A, Unali G, Conti A, Canarutto D, Albano L, Calabria A, Vavassori V, Cipriani C, Castiello MC, Esposito S, Brombin C, Cugnata F, Adjali O, Ayuso E, Merelli I, Villa A, Di Micco R, Kajaste-Rudnitski A, Montini E, Penaud-Budloo M, Naldini L. Choice of template delivery mitigates the genotoxic risk and adverse impact of editing in human hematopoietic stem cells. Cell Stem Cell. 2022 29:1428-1444.e9.
21. Li Z, Wang X, Janssen JM, Liu J, Tasca F, Hoeben RC, Gonçalves MAFV. Precision genome editing using combinatorial viral vector delivery of CRISPR-Cas9 nucleases and donor DNA constructs. Under review.
22. Suchy FP, Karigane D, Nakauchi Y, Higuchi M, Zhang J, Pekrun K, Hsu I, Fan AC, Nishimura T, Charlesworth CT, Bhadury J, Nishimura T, Wilkinson AC, Kay MA, Majeti R, Nakauchi H. Nat Biotechnol. 2024. doi: 10.1038/s41587-024-02171-w. Online ahead of print.
23. Flotte TR, Solow R, Owens RA, Afione S, Zeitlin PL, Carter BJ. Gene expression from adeno-associated virus vectors in airway epithelial cells. Am. J. Respir. Cell. Mol. Biol. 1992 7:349-356.
24. Haberman RP, McCown TJ, Samulski RJ. Novel transcriptional regulatory signals in the adeno-associated virus terminal repeat A/D junction element. J. Virol. 2000 74:8732-8739.
25. Bazick HO, Mao H, Niehaus JK, Wolter JM, Zylka MJ. AAV vector-derived elements

integrate into Cas9-generated double-strand breaks and disrupt gene transcription. Mol. Ther. 2024 S1525-0016(24)00656-7. doi: 10.1016/j.ymthe.2024.09.032. Online ahead of print

26. Schiroli G, Conti A, Ferrari S, Della Volpe L, Jacob A, Albano L, Beretta S, Calabria A, Vavassori V, Gasparini P, Salataj E, Ndiaye-Lobry D, Brombin C, Chaumeil J, Montini E, Merelli I, Genovese P, Naldini L, Di Micco R. Precise Gene Editing Preserves Hematopoietic Stem Cell Function following Transient p53-Mediated DNA Damage Response. Cell Stem Cell. 2019 24:551-565.e8.
27. Allen D, Weiss LE, Saguy A, Rosenberg M, Iancu O, Matalon O, Lee C, Beider K, Nagler A, Shechtman Y, Hendel A. High-Throughput Imaging of CRISPR- and Recombinant Adeno-Associated Virus-Induced DNA Damage Response in Human Hematopoietic Stem and Progenitor Cells. CRISPR J. 2022 5:80-94.
28. Maggio I, Gonçalves MA. Genome editing at the crossroads of delivery, specificity, and fidelity. Trends Biotechnol. 2015 33:280-291.
29. Pavani G, Amendola M. Targeted Gene Delivery: Where to Land. Front Genome Ed. 2021 2:609650. Corrigendum: Front Genome Ed. 2021 3:682171.
30. Spector LP, Tiffany M, Ferraro NM, Abell NS, Montgomery SB, Kay MA. Evaluating the Genomic Parameters Governing rAAV-Mediated Homologous Recombination. Mol Ther. 2021 29:1028-1046.
31. Bijlani S, Pang KM, Sivanandam V, Singh A, Chatterjee S. The Role of Recombinant AAV in Precise Genome Editing. Front Genome Ed. 2022 3:799722.
32. Holkers M, de Vries AA, Gonçalves MA. Nonspaced inverted DNA repeats are preferential targets for homology-directed gene repair in mammalian cells. Nucleic Acids Res. 2012 40:1984-1999.
33. Holkers M, Maggio I, Henriques SF, Janssen JM, Cathomen T, Gonçalves MA. Adenoviral vector DNA for accurate genome editing with engineered nucleases. Nat Methods. 2014 11:1051-1057.
34. Medert R, Thumberger T, Tavhelidse-Suck T, Hub T, Kellner T, Oguchi Y, Dlugosz S, Zimmermann F, Wittbrodt J, Freichel M. Efficient single copy integration via homology-directed repair (scHDR) by 5' modification of large DNA donor fragments in mice. Nucleic Acids Res. 2023 51:e14.
35. Brescia, M., *et al*., High-Capacity Adenoviral Vectors Permit Robust and Versatile Testing of DMD Gene Repair Tools and Strategies in Human Cells. Cells, 2020 9: 869.
36. Tasca F., Wang Q., Goncalves M Adenoviral vectors meet gene editing: a rising partnership for the genomic engineering of human stem cells and their progeny. Cells. 2020; 9:953.

37. Ricobaraza A., Gonzalez-Aparicio M., Mora-Jimenez L., Lumbreras S., Hernandez-Alcoceba R. High-capacity adenoviral vectors: expanding the scope of gene therapy. Int. J. Mol. Sci. 2020; 21:3643.
38. Wang Q, Liu J, Janssen JM, Le Bouteiller M, Frock RL, Gonçalves MAFV. Precise and broad scope genome editing based on high-specificity Cas9 nickases. Nucleic Acids Res. 2021 49:1173-1198.
39. Dever DP, Bak RO, Reinisch A, Camarena J, Washington G, Nicolas CE, Pavel-Dinu M, Saxena N, Wilkens AB, Mantri S, Uchida N, Hendel A, Narla A, Majeti R, Weinberg KI, Porteus MH. CRISPR/Cas9 β-globin gene targeting in human haematopoietic stem cells. Nature. 2016 539:384-389.
40. Pavani G, Fabiano A, Laurent M, Amor F, Cantelli E, Chalumeau A, Maule G, Tachtsidi A, Concordet JP, Cereseto A, Mavilio F, Ferrari G, Miccio A, Amendola M. Correction of β-thalassemia by CRISPR/Cas9 editing of the α-globin locus in human hematopoietic stem cells. Blood Adv. 2021 5:1137-1153.
41. McColl-Carboni A, Dollive S, Laughlin S, Lushi R, MacArthur M, Zhou S, Gagnon J, Smith CA, Burnham B, Horton R, Lata D, Uga B, Natu K, Michel E, Slater C, DaSilva E, Bruccoleri R, Kelly T, McGivney JB 4th. Analytical characterization of full, intermediate, and empty AAV capsids. Gene Ther. 2024 31:285-294.
42. Frock RL, Hu J, Meyers RM, Ho YJ, Kii E, Alt FW. Genome-wide detection of DNA double-stranded breaks induced by engineered nucleases. Nat. Biotechnol. 2015 33:179-186.
43. Kosicki M, Tomberg K, Bradley A. Repair of double-strand breaks induced by CRISPR-Cas9 leads to large deletions and complex rearrangements. Nat Biotechnol. 2018 36:765-771.
44. Lombardo A, Cesana D, Genovese P, Di Stefano B, Provasi E, Colombo DF, Neri M, Magnani Z, Cantore A, Lo Riso P, Damo M, Pello OM, Holmes MC, Gregory PD, Gritti A, Broccoli V, Bonini C, Naldini L. Site-specific integration and tailoring of cassette design for sustainable gene transfer. Nat. Methods 2011 8:861-869.
45. Ihry RJ, Worringer KA, Salick MR, Frias E, Ho D, Theriault K, Kommineni S, Chen J, Sondey M, Ye C, Randhawa R, Kulkarni T, Yang Z, McAllister G, Russ C, Reece-Hoyes J, Forrester W, Hoffman GR, Dolmetsch R, Kaykas A. p53 inhibits CRISPR-Cas9 engineering in human pluripotent stem cells. Nat Med. 2018 24:939-946.
46. Chen X, Tasca F, Wang Q, Liu J, Janssen JM, Brescia MD, Bellin M, Szuhai K, Kenrick J, Frock RL, Gonçalves MAFV. Expanding the editable genome and CRISPR-Cas9 versatility using DNA cutting-free gene targeting based on in trans paired nicking. Nucleic Acids Res. 2020 48:974-995.

47. Wang Q, Liu J, Janssen JM, Gonçalves MAFV. Precise homology-directed installation of large genomic edits in human cells with cleaving and nicking high-specificity Cas9 variants. Nucleic Acids Res. 2023 51:3465-3484.